IDA

INSTITUTE FOR DEFENSE ANALYSES

Ionospheric Scintillation Effects on a Space-Based, Foliage Penetration, Ground Moving Target Indication Radar

M. T. Tuley
T. C. Miller
R. J. Sullivan

August 2001

IDA Document D-2579
Log: H 01-000481

This work was conducted under contract DASW01 98 C 0067, DARPA Assignment DA-2-155, for DARPA/SPO. The publication of this IDA document does not indicate endorsement by the Department of Defense, nor should the contents be construed as reflecting the official position of that Agency.

INSTITUTE FOR DEFENSE ANALYSES

IDA Document D-2579

Ionospheric Scintillation Effects on a Space-Based, Foliage Penetration, Ground Moving Target Indication Radar

M. T. Tuley
T. C. Miller
R. J. Sullivan

PREFACE

This study was undertaken as part of a DARPA seedling effort to evaluate the potential feasibility of space-based operation of a foliage-penetrating radar capable of ground moving-target detection. Per our tasking, the analysis focused narrowly on the effects of atmospheric scintillation on the operation of such a radar, although to provide quantitative examples of scintillation effects, a strawman radar system was postulated. MIT Lincoln Laboratory undertook the more general study of orbits, constellations and radar resource requirements.

The authors would like to acknowledge the sponsorship and direction provided by Mr. Lee Moyer of DARPA. His suggestions concerning approach and the questions he posed in interim briefings of this work were extremely helpful. In addition, the careful review and comments of Dr. James Ralston, the IDA Task Leader for foliage-penetration work, are greatly appreciated.

CONTENTS

FIGURES

TABLES

EXECUTIVE SUMMARY

This report provides the results of a brief study of the possible effects of ionospheric scintillation on a space-based, foliage-penetration (FOPEN), ground moving-target indication (GMTI) radar operating in the ultrahigh-frequency (UHF) band. The results of publicly available data and analyses are applied to a specific strawman FOPEN space-based radar (SBR) system operating from low-Earth orbit. Performance degradations due to ionospheric scintillation and a combination of ionospheric scintillation and internal clutter motion caused by wind are calculated for a 3 m/s target minimum detectable velocity (MDV) at 15-deg grazing, point parameters felt to be minimally acceptable for an operational system. Space-time adaptive processing (STAP) is used to provide the clutter rejection necessary for successful performance. The analysis shows that significant radar resources (antenna size and average power) are needed to provide acceptable performance for a STAP-based system in the absence of scintillation or clutter internal motion. That would argue that a synthetic aperture radar (SAR)-based GMTI approach might be more attractive. However, the long dwell times required for SAR would exacerbate detrimental scintillation effects, so we feel that an analysis of a STAP-based approach provides a reasonable baseline on which to judge a FOPEN GMTI concept.

For UHF radar systems, the effects of scintillation can generally be summarized geographically as follows:

- Between 20-deg and 55-deg latitudes, scintillation should have little or no effect on STAP-based radar operation, except during periods of highest solar activity. Even then, the effects are likely to be small. SAR-based systems could see some effects during normal solar activity and are likely to be adversely affected during peak solar activity.
- Between ±20-deg latitude, there will be some adverse effects on radar operation most nights between local sunset and local sunrise. For a SAR-based system, those effects would likely significantly degrade operation at least half the time (and perhaps as much as 90 percent of the time). During the local day, effects should be negligible, except during solar activity maximums.

- Between 55-deg and 70-deg latitudes, there will be significant adverse effects on radar operation during local winter. During local summer, effects should be more similar to those at mid-latitudes, except during solar maximums.
- Between 70-deg and 90-deg latitudes, effects will extend to most of the year, with local winter effects nearly as bad as nighttime effects near the equator, but with local summer effects significantly less severe. Even summertime effects, however, may be significant enough to cause marginal operation of SAR-based GMTI systems, particularly when waveform distortion effects are included, along with decorrelation of target and clutter.

1. INTRODUCTION

The ionosphere is the region of the atmosphere extending from approximately 50 km to several hundred kilometers in altitude. Its most notable feature is its partial ionization by solar radiation. The resulting free electrons are responsible for the reflection and refraction of signals that allows long-range, high-frequency (HF) radio communications. Another effect, of great interest when attempting to detect and track objects on the ground from a space-based radar (SBR), is ionospheric scintillation. Ionospheric scintillation is due to rapid fluctuations in electron density in a disturbed or irregular patch of ionosphere along the path between the radar and the object of interest. The resulting changes in the index of refraction cause changes in the velocity and direction of travel of radio-frequency signals, resulting in parts of a signal arriving out of phase or being reflected into or out of the beam aimed at the observer. There are three primary types of scintillation:

1. *Intensity scintillation.* Signal power being scattered into or out of the line of sight of the observer.
2. *Angular scintillation.* Scattered radiation appearing to come from a direction different from the true direction to the target.
3. *Phase scintillation.* Time- and frequency-dependent changes in propagation velocity that cause the phase of the received signal to fluctuate in time.

In this document, we focus on the direct effects of a combination of intensity and phase scintillation, as defined through the decorrelation properties of the signal's mutual coherence function.

The magnitude of scintillation effects depends upon many factors. Causes for the observed effects are discussed in more detail in subsequent sections of the report:

1. *Latitude.* Signal degradation due to scintillation is most significant within 10 deg of the magnetic equator, least at mid-latitudes, and intermediate at high latitudes (above 55 to 60 deg). Scintillation effects appear to be more irregular and more difficult to accurately predict at the poles than near the equator.
2. *Longitude.* Widely separated sites at the same latitude can have very different scintillation levels. For example, differences are observed when comparing data from receiving stations in Alaska and Greenland or Kwajalein and Peru.

3. *Time of day.* In the equatorial zone, scintillation effects are generally worst from sunset to about midnight. At polar latitudes, scintillation appears to occur at any time of day or night.

4. *Season.* Scintillation effects also show a seasonal distribution. For example, equatorial scintillation is worse from February to October, but polar scintillation is worse during the local winter months.

5. *Solar cycle.* Scintillation magnitude depends strongly on solar cycle. At solar maximum, when the number of sunspots is greatest and solar activity is highest, scintillation effects are the worst. Solar maxima occur approximately every 11 years, with the next two due in late 2001 and 2012.

6. *Frequency.* All scintillation effects appear to be strongly frequency dependent. Most effects are much worse at longer wavelengths. So scintillation typically is very bad at very high frequencies (VHF), significant at ultra-high frequencies (UHF), of concern at L-Band, and almost never noticeable at X-band. HF radars are not included in this study because the same ionospheric effects that make them suitable for over-the-horizon operation also make them unsuitable for space-based operation.

7. *Atmospheric disturbances.* Severe atmospheric disturbances, such as high-altitude nuclear explosions, can greatly increase scintillation activity.

The purpose of this report is to characterize the potential impact of ionospheric scintillation on the performance of an SBR designed to detect moving targets under trees. To accomplish that purpose, we have calculated the performance of a strawman radar design and the degradation caused by ionospheric scintillation. In addition, a combination of ionospheric scintillation and internal clutter motion caused by the wind is also analyzed to evaluate a situation that will often arise. Although evaluation of effects through the use of a strawman system may not lead to the most general results, it does provide a concrete, illustrative example of the degraded performance that might be seen.

Section 2 provides an explanation of scintillation metrics and describes the spatial and temporal properties of ionospheric scintillation. Section 3 briefly outlines the results of a literature search undertaken to obtain data on scintillation and its effects. Section 4 provides an overview of the model used to predict the effects of scintillation on radar performance and details changes made to the model to handle scintillation effects. Section 5 provides performance results, and Section 6 contains conclusions.

2. SCINTILLATION PROPERTIES AND EFFECTS

This section first describes the parameters normally used by the electromagnetic propagation community to quantify ionospheric scintillation and then describes how the parameters are applied to evaluate scintillation effects. Finally, spatial and temporal variations of ionospheric scintillation are explored.

Scintillation is caused by changes in the refractive index in the signal path due to inhomogeneities and irregularities in the ionosphere. Such irregularities are caused by complex interactions between Earth's magnetic field, incident solar flux, and fluid transport phenomena. The scintillation that might affect a UHF SBR is due mostly to the rapid motion of the radar line-of-sight through ionospheric inhomogeneities that could have overall sizes of the order of hundreds of kilometers, but smaller scale internal structure of the order of a few kilometers or less. It is not the purpose of this report to explore the detailed physics of the ionosphere. Instead, we focus on scintillation effects on radar, with some support from equations that illustrate expected trends of the scintillation.

2.1 SCINTILLATION MEASURES

Under conditions of fading due to scintillation activity, it is convenient to express the received power as (Ref. 1)

$$S_r = S_0 S \sigma / \langle \sigma \rangle \quad , \tag{1}$$

where S_r is the power received in a given radar pulse, S_0 is the mean signal power received from the target, S is the fractional change due to scintillation activity, and $\sigma/\langle\sigma\rangle$ is the fractional change in received power due to target cross-section fluctuations. Since the signal variations due to target and scintillation effects are independent, the total signal fluctuation can be expressed simply as their product, and we can examine each part separately. Here, we focus only on the scintillation effects.

S_4, sometimes called the scintillation index, is a standard measure of the severity of the power fluctuations due only to scintillation and is defined as

$$S_4^2 = \frac{\left\langle \left(S - \langle S \rangle\right)^2 \right\rangle}{\langle S \rangle^2} \quad . \tag{2}$$

Thus, S_4 is the standard deviation of the fluctuation caused by scintillation, normalized by the mean value of the scintillation fluctuation. Note that in practice one cannot measure S directly, but only the received power P. One must then attempt to remove other effects causing fluctuations or trends. In fact, S_4 is usually defined with P substituted for S in Equation (2), but with the assumption that one has removed all other fluctuations and trends.

An S_4 value of zero represents a constant signal, one with no fading. In contrast, $S_4 = 1$ implies saturated scintillation, where the in-phase *(I)* and quadrature *(Q)* components of the received signal are uncorrelated, zero-mean, Gaussian random variables. Values of S_4 exceeding unity are sometimes observed in the data (see, e.g., Figure 3). Such values are indicative of focusing, which is caused by large-scale irregularities (Ref. 2).

Fremouw et al. (Ref. 3) have concluded that the distribution of the signal power due to scintillation is best described by a Nakagami *m*-distribution, so that the probability density for S on a one-way path from the target to the observer for a given S_4 is given by:

$$p_1(S)dS = \frac{m^m S^{m-1}}{\Gamma(m) < S >^m} \exp\left(\frac{-mS}{< S >}\right) dS \quad , \tag{3}$$

where $m = 1/S_4^2$. For S_4 close to zero, the Nakagami distribution becomes a narrow Gaussian of mean one. As S_4 approaches one, the distribution becomes exponential, as would be expected for uncorrelated Gaussian I and Q.

For the case of a monostatic radar, the signal propagates twice over the same path, passing through identical irregularities (assuming that the fluctuation time is much longer than the propagation time, which is true for all cases of interest here). So we can substitute $Q = S^2$ for the two-way case to obtain:

$$p_2(Q)dQ = \frac{\left[m(m+1)\right]^{m/2} Q^{m/2-1}}{2\Gamma(m) < Q >^{m/2}} \exp\left(-\sqrt{\frac{m(m+1)Q}{< Q >}}\right) dQ \quad . \tag{4}$$

The received power distribution is not used directly in the performance predictions presented here. Instead, target and clutter fluctuations due to scintillation are approached indirectly through the temporal correlation properties of their signals. For the clutter, the spatial and temporal covariance matrix determines the success with which the

space-time adaptive processing (STAP) algorithms can successfully cancel clutter that would otherwise compete with the target. For the target, the assumption is normally made that no fluctuations occur during a coherent processing interval (CPI). In this case, we use the temporal decorrelation properties to determine integration loss due to scintillation.

2.2 TEMPORAL CORRELATION

The effect of scintillation on signal strength does not vary randomly on arbitrarily short time scales. The values of S at any two times are correlated, with the degree of correlation depending on the time between the measurements because the scintillation causes the signal to fade in and out over time. Correlation properties become very important when either STAP or synthetic aperture radar (SAR) processing is employed for target detection. As noted earlier, STAP processing depends on the correlation of both clutter and target over a CPI. SAR processing similarly depends on the correlation of the target for coherent gain over the image formation time.

The signal decorrelation time, τ_0, is a metric that describes the fading rate of the received signal during scintillation. It is defined as the time separation, τ, at which the magnitude of the mutual coherence function reaches the value of $1/e$. For strong scattering, the mutual coherence function can be modeled as Gaussian and so is given by (Ref. 2)

$$\left\langle E^*(t+\tau)E(t)\right\rangle = \left\langle \left|E(t)^2\right|\right\rangle \exp\left(-\tau^2/\tau_0^2\right) \quad , \tag{5}$$

where E is the received voltage and $<|E(t)|^2>$ is the average received power.

The inverse of the fading rate or fading bandwidth is τ_0. Large values of τ_0 correspond to slow fading conditions and small values correspond to fast fading. In this effort, we are mostly concerned with fading effects within a CPI, and so small values of τ_0 are of most concern.

The expression for τ_0 is given by (Ref. 4)

$$\tau_0 = \frac{L_0}{\sqrt{\ln(L_0/l_i)}\sigma_\phi v_L} \quad , \tag{6}$$

where

$$\sigma_\phi^2 = 2(r_e\lambda)^2 L_0 L\left(\Delta N_e^2\right) \quad , \tag{7}$$

and r_e is the classical electron radius, L is the thickness of an ionized layer, ΔN_e^2 is the variance of electron density irregularities, λ is the radar wavelength, L_0 is the outer scale

size and l_i is the inner scale size for the dimension of the irregularities in the atmosphere, and v_L is the velocity of the line-of-sight along the direction of L.

Combining Equations (6) and (7) gives the prediction that decorrelation time should be proportional to radar frequency. Data from the Wideband Satellite experiment, described in Section 3.2, supports this prediction (see Figure 1). As can be seen, 50 percent of the time, fade times are typically a few tenths of a second at UHF frequencies, and 90 percent of the time they are shorter than 2 seconds. Figure 1 also illustrates the difficulties in going to frequencies lower than UHF if reasonably long CPIs will be required to provide sufficiently narrow Doppler filters. In such cases, signal coherence time might be shorter than the CPI.

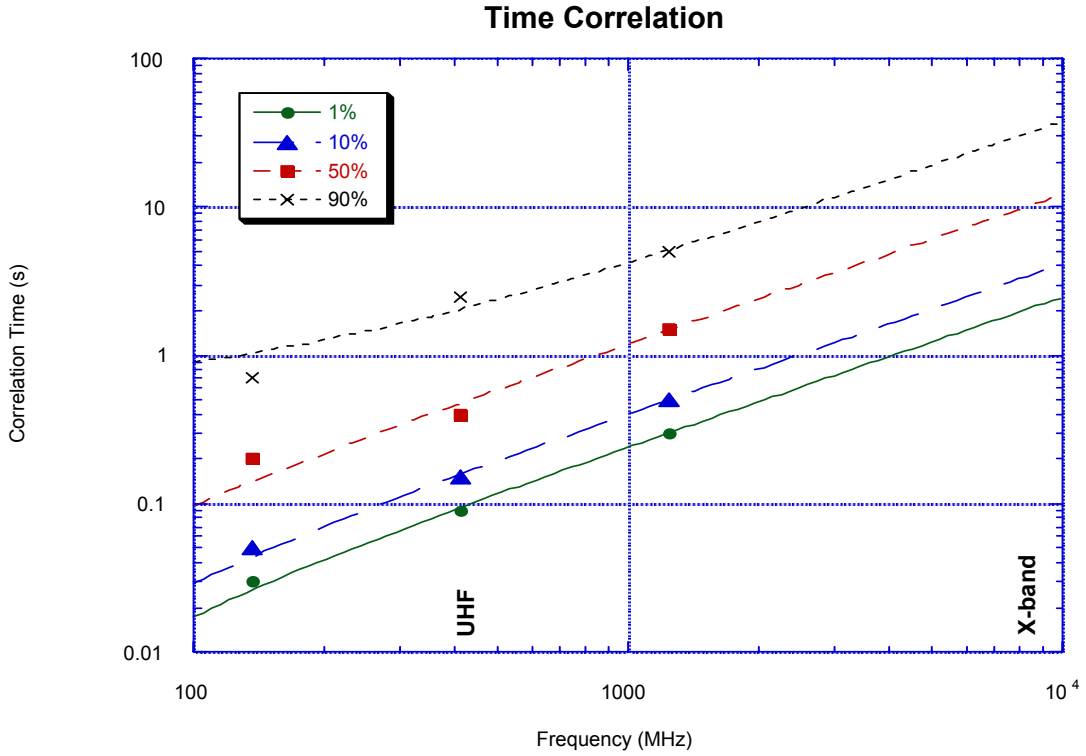

Figure 1. Signal Decorrelation Time vs. Frequency (Ref. 4), at Several Different Maximum Cumulative Occurrence Levels, with Linear Fits

2.3 FREQUENCY CORRELATION

Scintillation effects are correlated in frequency as well as time. The channel coherence bandwidth, f_{coh}, describes the maximum bandwidth over which S values will be strongly correlated, as given in Equations (8) and (9) (Ref. 1), and includes both temporal and frequency effects on the complex mutual coherence function:

$$\left\langle E(t+\tau, f+f_d)E^*(t,f)\right\rangle = |E_0|^2 \exp\left(\frac{-\tau^2/\tau_0^2}{1+if_d/f_{coh}}\right)(1+if_d/f_{coh})^{-1} \quad , \tag{8}$$

$$f_{coh} = \frac{\pi c(z_t+z_r)L_0}{\sqrt{2}r_e^2\lambda^4 \ln(L_0/l_i)z_t z_r L\overline{\Delta N_e^2}} \quad , \tag{9}$$

where f_d is the frequency excursion, c is the speed of light in vacuum, z_t is the distance from the transmitter to the center of the ionized layer causing the scintillation, $z_t + z_r$ is the total one-way propagation distance, and i is the imaginary operator.

The dispersion caused by the ionosphere has two main effects. First, a single pulse of greater bandwidth will show undesired pulse distortion due to different signal-frequency components undergoing unequal attenuation. After receiver processing, such distortion often results in degraded time-domain sidelobes and decreased signal-processing gain. Second, it provides a measure of the effectiveness of using multiple frequencies to mitigate scintillation effects. For example, sequential CPIs could be transmitted at two frequencies using a frequency-agile radar, with each pulse within a CPI having an instantaneous bandwidth less than f_{coh} but with the two CPI frequencies separated by more than f_{coh}. Fading of the two signals would be uncorrelated, increasing the probability that detection could be maintained through noncoherent integration of multiple CPIs.

Knepp and Reinking (Ref. 1) provide measurements of f_{coh} using Wideband Satellite data and show an average f_{coh} of 34 MHz at UHF frequencies. This is about the same width as the allocated UHF radar band (420–450 MHz). Therefore, making uncorrelated measurements at different UHF frequencies within this band will probably not be possible during scintillation, and other mitigation strategies will have to be investigated if scintillation decorrelation is to be employed in signal processing.

One can extrapolate f_{coh} to higher and lower frequencies using the λ^{-4} relationship given in Equation (9). At VHF frequencies, f_{coh} is only a few megahertz, implying that narrowband frequency-agile radars would be effective for improving performance in this regime during scintillation, but that wideband operation would be difficult. At X-band, f_{coh} is much greater than the maximum possible bandwidth; however, scintillation levels are so low at X-band that frequency-agile operations should not be necessary for scintillation decorrelation, although they might still be useful for decorrelation of target fluctuation effects.

2.4 SCINTILLATION PROBABILITY OF OCCURRENCE

Given a value of S_4, we can determine the character of the scintillation through the amplitude distribution and τ_0. The more difficult task is to define the S_4 probability density distribution for a given location, time, season, point in solar cycle, and frequency. Unfortunately, the large number of factors that affect S_4 make it very difficult to find this probability distribution for any given set of conditions. Only a limited number of experiments have been carried out, and only selected subsets of data from them have been analyzed. As discussed below, there is at least one very extensive model, WBMOD, for predicting S_4 values as a function of all of the inputs above. However, it is proprietary software, and the developer charges for its use. In any event, exercise of such a sophisticated modeling package is not considered necessary for the purpose of this study, where general scintillation conditions are of interest, not location and time-specific predictions as would be provided by WBMOD.

2.4.1 Temporal and Spatial Distributions of Scintillation

Ionospheric scintillation is a phenomenon that varies widely with latitude, longitude, time of day, and level of solar activity. To simplify description, investigators often separate Earth into three latitude zones and categorize effects according to those zones (see Figure 2). The regions are the equatorial, high latitude, and middle latitude.

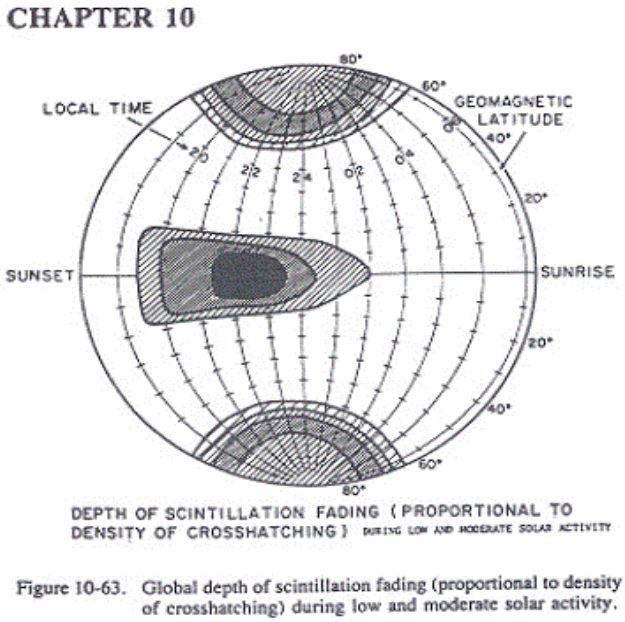

Figure 2. Illustration of the Geographic Distribution of Ionospheric Scintillation (Source: Ref. 5)

The equatorial region stretches ±20 deg around the magnetic equator, but has its highest intensity within 10 deg of the equator. The high-latitude region may stretch as far from the magnetic poles as 45 deg corrected geomagnetic latitude, but more often is restricted to above 55 deg. Middle-latitude scintillation is not as widely studied as the other two regions because the intensity is not as great; however, activity levels at VHF and UHF frequencies at mid-latitudes may be sufficient to increase error rates on communications systems with low fade margins (Refs. 6, 7).

Note from Figure 2 that significant equatorial region scintillation occurs after local sunset and before local sunrise. Although longitude, season, and solar activity can affect the details, a slice through Figure 2 at the equator provides a good indication of the temporal behavior of the scintillation. That is, scintillation activity will begin a slow build-up around 1800 local time, with a steeper slope beginning about 2000. Activity peaks between 2200 and midnight, then slowly decays. Sometimes, a second, but lower, peak can occur around 0600. Levels reached have a seasonal dependence, with maximums occurring during equinoctial months. Levels during periods of high sunspot activity similarly tend to be higher than when sunspot activity is moderate or low.

High-latitude ionospheric scintillation shows less of a diurnal pattern than that of the equatorial region; however, a definite seasonal pattern exists, with maximums occurring during the months with little or no sunlight. As with the equatorial region, high-latitude scintillation is exacerbated by increased solar activity.

2.4.2 Scintillation Levels

In exploring scintillation characteristics, we focus on equatorial and high-latitude scintillation because those are the areas where scintillation effects are likely to significantly degrade the performance of a foliage-penetration (FOPEN), ground moving-target indication (GMTI) SBR. If the system concept of operations does not require 24-hour-a-day operation between ±20 deg latitude around the magnetic equator or above approximately 50 deg latitude, then scintillation should not be a problem. In the performance predictions provided in Section 5, various levels of scintillation that might be expected at UHF are explored, with the goal to investigate how often given levels might be expected as a function of frequency.

The Wideband Satellite experiment (described in Section 3.2) provides the most comprehensive database we have found for the problem of interest. Figure 3 shows an example from Knepp and Mokole (Ref. 2) for Kwajalein data from 1979. Analogous probability distributions are provided for Ancon, Peru, and Kwajalein for a time period in

1977, but no data are analyzed from the Alaskan station instrumented for the experiment. All the distributions given in Knepp and Mokole are from approximately 50 satellite passes during which the worst scintillation episodes were observed and therefore represent a worst case scenario for those particular observations. On the other hand, the 1977 data were collected during a period of low solar activity and are thus representative of less severe equatorial scintillation. The combination of the 1977 and 1979 data provides a measure of the variation that might be expected in a high-scintillation region.

Note from Figure 3 that the VHF band is most strongly affected by scintillation. S_4 levels are typically around unity and sometimes even exceed that level. UHF is not as badly affected, but scintillation levels are often still severe. L-Band suffers much less effect from scintillation, but even there, S_4 levels are above 0.5 sufficiently often to cause concern, particularly for systems with little margin. In Section 4, other data from Ref. 2 are used to establish one-way decorrelation times for various probability levels of scintillation activity. Those one-way decorrelation times are converted into two-way times and used to assess performance degradation caused by target decorrelation and the spreading of the clutter spectrum.

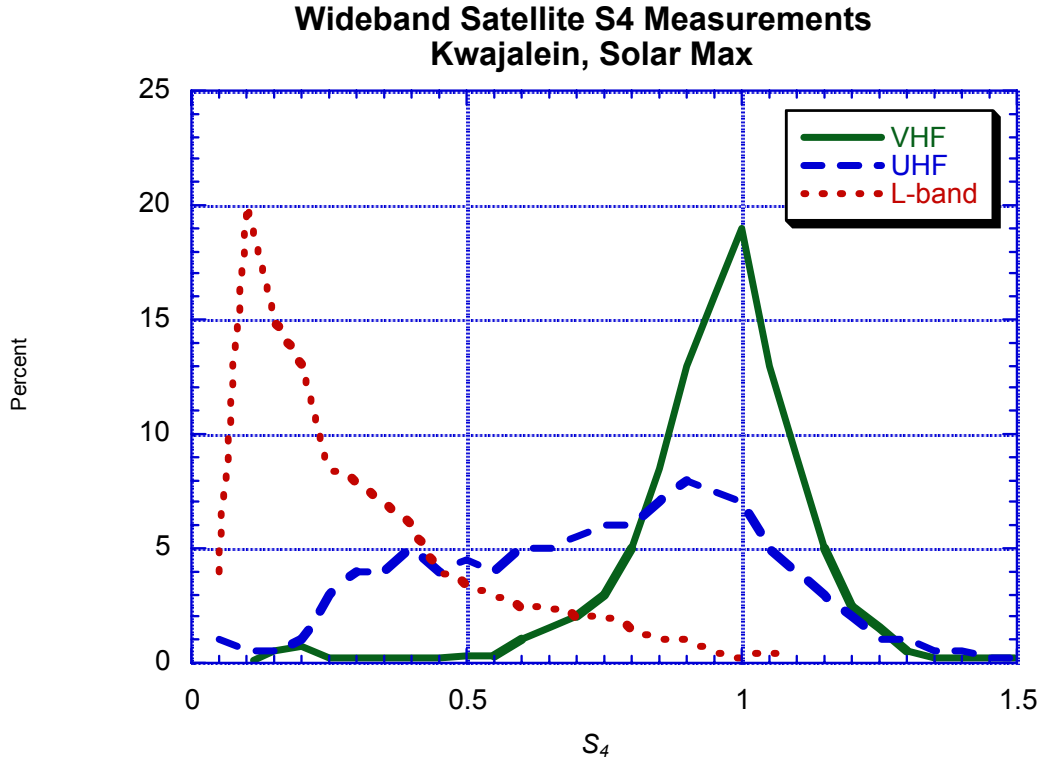

Figure 3. Example S_4 Distributions from Knepp and Mokole (Ref. 2) (Wideband Satellite Experiment Data) at Kwajalein During 1979 (Solar Maximum), for VHF, UHF, and L-band Frequencies

Figure 4 shows a rough comparison of the results from the Wideband Satellite experiment for average S_4 index as a function of solar activity and location (Refs. 2, 8, 9). Basu et al. (Ref. 9) present Alaskan data for what they term "quiet" and "disturbed" magnetic fields as a function of time of day and invariant latitude L [described by McHwain (Ref. 10)]. Knepp and Mokole (Ref. 2) present data at Kwajalein during periods when scintillation is most active, and Livingston (Ref. 8) presents such data for average periods at Kwajalein. In Figure 4, we have chosen to plot the data of Knepp and Mokole and that of Basu et al. for their "disturbed" periods, all during solar maximum, to compare relatively high scintillation levels at the various locations, even though the selection methods of the two papers are certainly somewhat different. With these caveats in mind, we can nevertheless make some tentative conclusions from the plot.

First, the polar scintillation level is dependent upon latitude (i.e., 70-deg latitude scintillation is worse than 58-deg latitude scintillation), implying that a detailed consideration of target and radar location must be taken into account. Second, at VHF the worst equatorial scintillation appears to be greater than even the highest latitude polar scintillation, implying that using equatorial scintillation data should result in a worst case study. Note, however, that the worst case Alaska solar max data is only slightly less severe than Kwajalein during solar max. Thus, near-polar scintillation cannot be ignored. Third, the drop-off of scintillation level with frequency is very strong. If the points in Figure 4 are extrapolated to X-band, then the S_4 index should always be below 0.1. Thus, an SBR concept such as Discoverer 2, operating at X-Band, likely would not be adversely affected by scintillation, even during periods of maximum activity. For FOPEN, however, we are forced to work at lower frequencies, and thus a system design must sometimes deal with scintillation effects. Note from Figure 4 that the average value of S_4 at Kwajalein, even during solar average conditions, is still around 0.4, a level of concern for performance.

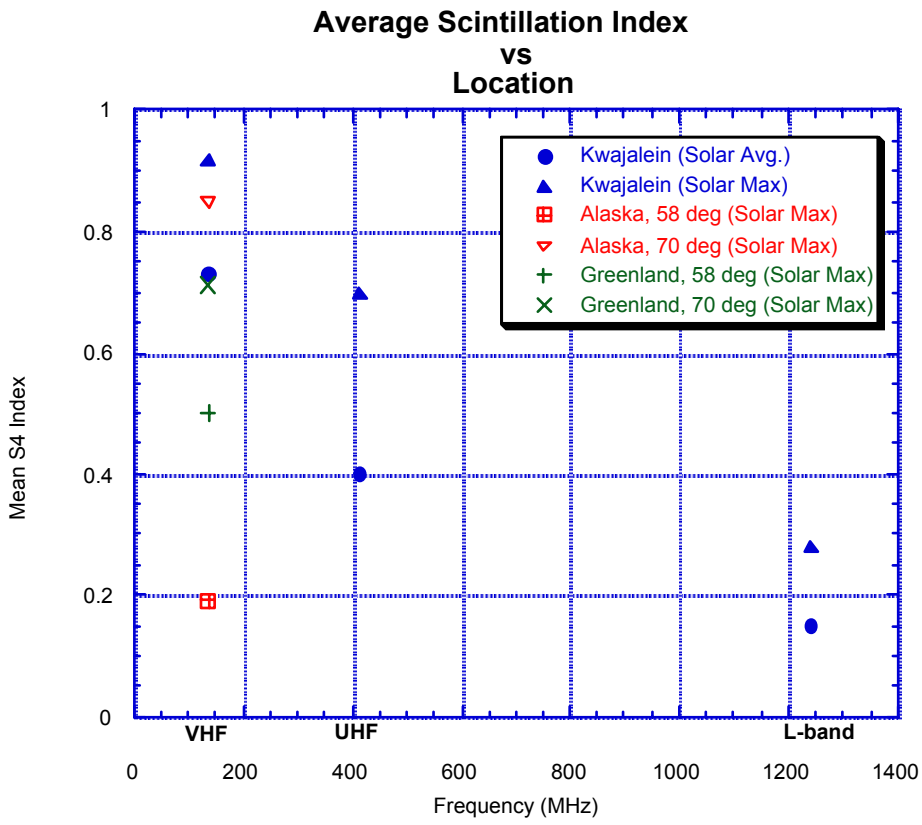

Figure 4. Scintillation Index vs. Frequency and Solar Cycle at Equatorial and Northern Polar Latitudes

3. SCINTILLATION DATA AND MODEL DESCRIPTIONS

Given the lack of a single comprehensive database, the primary purpose of this section is to list the various sources of scintillation data in the literature and give short descriptions of the possible utility of each. Although only some of the sources are used in our radar performance modeling, all that might be of potential use in any future studies of FOPEN GMTI systems operating from space are described. We intend for this to serve as a useful starting point and reference to researchers doing more detailed analyses in the future, if those prove necessary.

It is also worthwhile to point out that two basic types of ionospheric scintillation measurements have been made: those with an artificially disturbed ionosphere (*active* programs) and those measuring the natural ionosphere (*passive* programs). As we mentioned above, scintillation activity can be highly affected by atmospheric disturbances, and several research programs have used high-power, HF transmitters to cause artificial disturbances in the ionosphere. For SBR FOPEN GMTI purposes, we will assume that the case of most interest is that of the natural ionosphere, since most potential adversaries would have no means to provide large-scale disturbance of the ionosphere within the line of sight (LOS) of a constellation of SBRs using high-power transmitters. One obvious exception is the case of an enemy disturbing the ionosphere with a large, high-altitude, nuclear explosion. Currently, this scenario is beyond the scope of this work, except insofar as we have analyzed cases with very high S_4 values ($S_4 \sim 1$). In the following sections, we point out which measurements were made with active systems because the disturbed ionosphere in these cases is qualitatively different from the natural ionosphere, and, at best, some extrapolations must be made to apply the results to the passive, or natural, case.

3.1 HF ACTIVE AURORAL RESEARCH PROGRAM (HAARP), AIR FORCE RESEARCH LABORATORY (AFRL) EFFORTS

HAARP, begun in 1990, is collecting data on many ionospheric effects in Alaska. AFRL and the Office of Naval Research (ONR) jointly manage HAARP. The project is described quite well on their Web page (www.haarp.alaska.edu), and one of the many instruments being deployed will make VHF/UHF ionospheric scintillation measurements.

Unfortunately, their links to scintillation data were not operational during this study, and our inquiries did not lead to any scintillation data. HAARP should be a good source of scintillation data in a location of interest over the next several years.

AFRL is also developing the Communication/Navigation Outage Forecasting System (C/NOFS), using HAARP and other data sources. It is designed to forecast scintillation activity 4 to 24 hours in advance and provide warning of upcoming severe episodes. It appears to be similar to their existing Scintillation Network Decision Aid (SCINDA), except that SCINDA only works for equatorial locations; C/NOFS is apparently designed to work worldwide. The two projects are described on the AFRL Web site (www.vs.afrl.af.mil).

3.2 WIDEBAND SATELLITE EXPERIMENT

The Defense Nuclear Agency (DNA) Wideband Satellite experiment (Ref. 11) was launched in May 1976 into a polar orbit of 1,030-km altitude. It was used to study transionospheric signal propagation with a multifrequency beacon. Signals at 10 frequencies, ranging from VHF (137 MHz) to S-band (2,891 MHz), were recorded at stations at Kwajalein; at Ancon, Peru; near Chatanika, and Anchorage, Alaska; and in Goose Bay, Greenland. The satellite operated for 39 months, covering the solar maximum period in 1979. A number of authors (Refs. 2, 8, 9) have analyzed data from this experiment, and we have already cited some of that work in Section 2.4.2; however, all research appears to have concentrated on particular locations, times, or wavelengths. We were unable to find a survey paper giving S_4 distributions for all receiving locations at all times for all 10 wavelengths.

For example, Livingston (Ref. 8) analyzes data from Kwajalein and Ancon and presents results over a full year of observations. He only gives very coarse distribution information, however, so only rough guesses of the average S_4 index over a year are possible. Basu et al. (Ref. 9) present Wideband data for Alaska (receiving station in Anchorage: 61.2 deg N, 149.9 deg W) and Greenland (receiving station in Goose Bay). Unfortunately, the full probability distributions are not presented, only the 50-percent and 90-percent levels, and only at one VHF wavelength. As can be seen in Figure 3, S_4 distributions tend not to be Gaussian, with asymmetries and long tails, so it is very difficult to model the probability density function based upon only two numbers. We could extrapolate the VHF averages to UHF frequencies and then use a normal distribution as a zeroth-order approximation, but we have chosen instead to provide results using

the available equatorial distributions. Since high-latitude scintillation tends to be less severe than equatorial, this should provide a worst case as a starting point.

3.3 ALTAIR, HILAT, AND POLAR BEAR

Several additional satellite studies of scintillation were made in the 1980's. DNA's PEAK (Propagation Effects Assessment—Kwajalein) experiment was conducted in August 1989. The ALTAIR VHF/UHF wide-bandwidth radar was used to track spherical satellites in low-Earth orbit (LEO) from Kwajalein (Ref. 12). The experiment's purpose was to collect radar data during what was considered the most severe propagation disturbances available naturally (equatorial and near the maximum of solar activity, much like the 1979 Wideband measurements). The HiLat and Polar Bear satellites were used in the mid 1980's as radar targets to provide high-latitude scintillation data in the VHF and UHF bands (Ref. 13). We did not find readily usable S_4 distributions from any of these more recent experiments in the literature and so did not use data from them directly in the following sections; however, data from all of them have been used in the WBMOD model, described next.

3.4 WBMOD MODEL AND SCINTMOD PROGRAM

The most fully developed model for predicting scintillation activity appears to be the empirical WBMOD/SCINTMOD model/program produced by Northwest Research Associates (NWRA). E.J. Fremouw, J. Secan, and several coworkers have developed the WBMOD model over the past three decades (Refs. 14–17). An early version from 1973 (Ref. 14) is fairly simple and easy to program onto a spreadsheet, but only predicts average S_4 values and then only to within a factor of 2 at best. Since then, the model has become much more sophisticated, using data from the Wideband, ALTAIR, HiLat, and Polar Bear experiments, with many observations from around the world at different periods of the solar cycle. WBMOD uses a collection of empirical models based upon these observations to describe the global distribution of ionospheric irregularities. It then uses a power-law, phase-screen, propagation model to predict intensity and phase scintillation effects on user-defined systems and geometries. The current version, now called SCINTMOD, predicts full S_4 probability distributions when given all of the parameters described in Section 2. The SCINTMOD code is owned by NWRA, who provide full ionospheric scintillation consultation services, including help in converting the SCINTMOD output into effects on user's systems. For this seedling study, we have not used SCINTMOD. Rather, we have arrived at decorrelation times based on the

Wideband Satellite experiment. If more detailed studies were to be warranted in the future, we would strongly recommend using SCINTMOD and involving NWRA through whatever subcontractor/consultant arrangement would be appropriate.

4. RADAR PERFORMANCE SIMULATION

Detection of ground-moving targets from any moving platform presents difficulties in signal processing because motion of the radar platform impresses Doppler shifts on the clutter that may cause a portion of it to appear in the same Doppler filter as the target. For fast-moving targets or slowly moving radar platforms, the competing clutter may be in the sidelobes of the antenna pattern, generally called the exoclutter case. If good antenna sidelobe control is maintained, exoclutter targets may not require additional processing beyond normal Doppler filtering because two-way sidelobe attenuation may put clutter levels below receiver noise. If the clutter that competes with the target return falls in the antenna mainbeam (the endoclutter case), a combination of spatial and temporal processing is generally required to allow detection. Such processing may be non-adaptive, but more generally is adaptive (STAP).

This section describes a simulation specifically designed to focus on an SBR using STAP to detect endoclutter targets. The basics of STAP are well documented in the literature (Ref. 18), so the focus here is on the specific approach and assumptions used to provide performance predictions in this effort.

4.1 PROGRAM DESCRIPTION

Calculating the GMTI performance of an SBR involves a significant amount of bookkeeping regarding satellite orbits and velocities, ranges, grazing angles, etc., in addition to standard radar range equation and STAP calculations. To allow concentration on the effects of ionospheric scintillation, performance prediction efforts began with existing Mathcad code that already implemented the basic computations for SBR performance. The code used is a modified version of a Mathcad program developed by Dr. Robert W. Miller, a consultant to the AFRL, to calculate performance for the TechSat 21 program (Ref. 19).

TechSat 21 assumes a constellation of microsatellites, the outputs of which are processed using STAP to provide GMTI performance. Although the ability the program provides to treat general antenna configurations is useful, the original program does not consider some phenomena that are important for the scintillation study. These phenomena include the effects of a realistic CPI data window to reduce Doppler sidelobes, the effects

of internal clutter motion, and the effects of scintillation on both the target and the clutter. In addition, for the long CPIs required for detection by a FOPEN GMTI SBR, processing the full number of degrees of freedom (DOF) available is not computationally practical. A more practical scheme is to use post-Doppler STAP in either beam space or element space. All of these modifications are discussed in Section 4.2; this section focuses on program assumptions that were not changed.

4.1.1 Doppler Ambiguities

An LEO satellite has a velocity relative to Earth's surface in excess of 7 km/s. Thus, there will be significant Doppler spread across the beam of any antenna pattern intercepting Earth's surface. For the strawman system explored for this task, Figure 5 provides an indication of that Doppler spread, normalized by the pulse-repetition frequency (PRF) of 400 Hz. The transmit antenna mainbeam is pointed normal to the satellite velocity vector and at a 15-deg grazing angle.

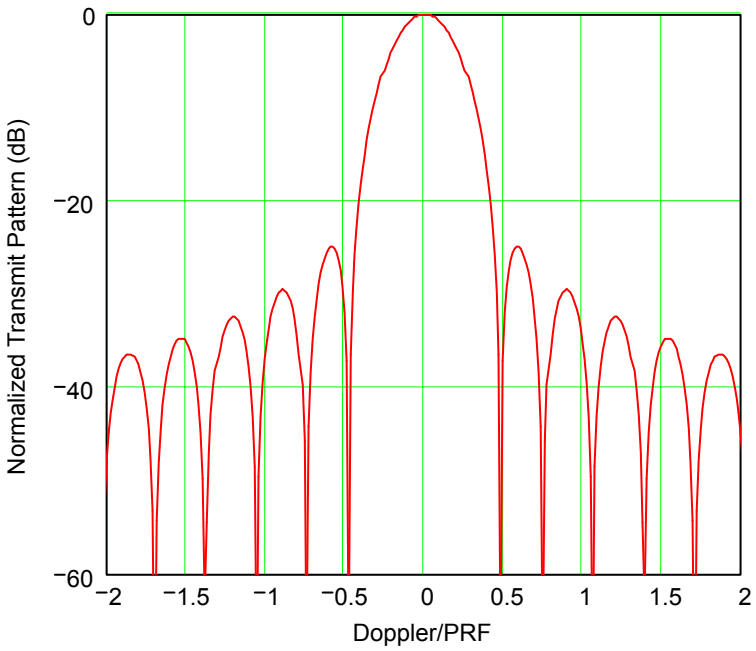

Figure 5. Normalized Transmit Pattern for the Strawman System as a Function of Doppler Frequency Normalized by the Radar PRF of 400 Hz

Note that the PRF has been chosen so that the first nulls of the antenna pattern lie inside the ± PRF/2 points to ensure that mainlobe clutter is unambiguous. Doppler is highly ambiguous outside the mainlobe, however. In an actual system, STAP would be used to cancel any sidelobe clutter that remained above the noise floor in the target Doppler filter, but would use up spatial DOF in the process. To reduce the computational

burden, we have ignored sidelobe clutter in this analysis. Predictions from our simulation show that the RCS of the mainlobe clutter competing with the target, before cancellation with STAP, is approximately 27 dBsm. The transmit antenna is modeled as having a one-parameter Taylor weighting, which gives a –25 dB first sidelobe. Clearly, additional processing is required to reduce clutter at the peak of the first sidelobe to below target level (particularly when foliage attenuation of the target signal is considered), much less to below noise. Spatial nulls placed in the sidelobes of the antenna pattern, however, result in little additional signal-processing loss, as long as sufficient spatial DOF are available. Assuming no additional loss is certainly optimistic. Nevertheless, because we show that adequate performance requires very large power-aperture products, even with optimistic assumptions, the results should be useful. If further investigation of such a design is desired, the restriction on considering only mainlobe clutter can be relaxed, albeit at the cost of increased computation.

4.1.2 Range Ambiguities

Range ambiguity, like Doppler ambiguity, provides additional clutter patches that compete with the target return. For an airborne platform operating against targets near zero grazing angle, range ambiguities will lie along a single azimuth line and thus can be canceled with a single spatial null. However, the strawman case taken here considers a 15-deg grazing angle. For angles that steep, subsequent range ambiguities may lie far enough off the azimuth line of the primary range cell competing with the target that additional spatial DOF are required to provide the appropriate null.

This problem is further complicated by SBR geometries. For the LEO altitude of 500 km chosen for this study, the range to the target is 1,407 km at 15-deg grazing. As noted above, a PRF of 400 Hz has been chosen, giving an unambiguous range interval of 374.7 km. The transmit antenna has been sized so that its mainlobe footprint (null-to-null) is shorter than an ambiguous range interval. Unlike a low PRF airborne system where all ambiguities are typically at ranges beyond the target, however, SBRs will typically have ambiguities at ranges inside the target. In this case, ambiguities appear at 657.6- and 1,032.3-km ranges (the first ambiguity at 282.9 km does not intersect the surface of Earth). The close-in ambiguities have higher received power because of the R^{-4} factor in the radar range equation. Although the decreased range will reduce the width of the clutter patch, the range law and increase in clutter radar cross-section per unit area with increasing grazing angle more than offset that effect.

Two methods are potentially available to deal with range ambiguities that lie between the radar and target. One that should be used, even if the other is also employed, is controlling the transmit beam elevation sidelobes to minimize illumination of close-in clutter patches. If that is not sufficient to reduce the competing clutter below noise, spatial nulls must be placed on the offending clutter. Those nulls can be formed in either the elevation or azimuth plane. Because of the proximity in azimuth of the competing clutter patches to the target, forming elevation nulls is preferred. Such an approach, however, requires STAP to be performed in the elevation plane, significantly increasing the processing burden and the number of receiver channels required.

In this effort, for range ambiguities as for Doppler ambiguities, we have ignored contributing clutter patches outside the mainlobe of the radar. As noted in the previous paragraph, such patches will likely require that STAP be applied to reduce their effects. Nevertheless, we can again argue that placing nulls outside the mainbeam of the radar, while a computational burden, should not markedly increase STAP losses. Thus, this approach with range ambiguities is reasonable, if somewhat optimistic.

4.2 PROGRAM MODIFICATIONS FOR SCINTILLATION CALCULATIONS

Although the TechSat 21 Mathcad program provided a very good framework around which to build performance predictions, some important effects were added for this effort: implementation of a realistic Doppler filter model, inclusion of pulse-repetition interval (PRI) stagger processing, provision for the effects of clutter internal motion, FOPEN losses, and scintillation effects. Each is described in the following subsections.

4.2.1 Doppler Filter Model

When a discrete Fourier transform (DFT) is performed on the samples from a CPI of radar data, the spacing between sample points in the frequency domain is given as 1/CPI. In the original version of the TechSat 21 program, that Doppler bin width was used to calculate the width of the clutter cell competing with the target. All of the clutter from the cell was assumed to be located at the center of the cell, and that angular location was used to calculate the appropriate path length (hence phase) of the clutter return in each of the antenna subapertures. In reality, even if no window is used on the CPI data to reduce Doppler sidelobes, the clutter return will exhibit a $\sin(x)/x$ behavior in the frequency domain. Generally, the –13.2 dB first sidelobes and slow falloff of the $\sin(x)/x$ function make it unattractive, hence the use of a Doppler window function.

We chose a 0.85 s CPI for the strawman system, resulting in a Doppler filter bin width of 1.2 Hz. At 435 MHz, that represents a Doppler bin width of just over 0.4 m/s. Figure 6 illustrates that width for a nominal Doppler filter centered at 5 m/s. Also shown in the figure is the transform of the Kaiser-Bessel window function that was used in these predictions to represent a realistic Doppler filter characteristic. The Kaiser-Bessel window, as described by Harris (Ref. 20), is the function of restricted time duration, T, that maximizes the energy in a band of frequencies, B. Sidelobes are determined by a factor, a, which is a function of the time-bandwidth product and which sets the level of the maximum sidelobe. In this effort, several values of a were explored. An $a = 2$ value, providing –46 dB first sidelobes, was chosen as a compromise between mainlobe width and sidelobe level. We chose the Kaiser-Bessel window because Harris lists it as one of the top-performing windows. A more common window such as Hann, Hamming, or Taylor could have been used instead; however, we do not believe the results obtained depend strongly on the window chosen.

In Figure 6, note that the width of the Kaiser-Bessel window is much wider than one Doppler filter width. Blackman lists the 3-dB width as 1.43 bins, but the null-to-null width is over 4 bins. The major effect of the increased width is to increase the width of the spatial null required to cancel clutter competing with the target. For very low velocity targets, such an increase in null width results in rapidly increasing STAP losses as the spatial null formed by STAP moves closer to the target location.

The effect of a realistic Doppler filter on performance is significant, even in the absence of scintillation or windblown clutter. Figure 7 provides predictions of signal-to-interference-plus-noise ratio (SINR) loss as a function of target radial velocity for target radial velocity for the theoretical, idealized bin width (rectangular Doppler filter) and for the practically realizable Kaiser-Bessel filter. SINR loss is defined as the SINR achieved after STAP divided by the SINR that would be achieved in a noise-only environment, that is, an environment with no clutter and no jammers.

Note the significantly smaller loss incurred by the (unphysical) rectangular filter at the lower radial velocity values. Below 5 m/s, the rectangular filter is approximately 10 dB better than the more realistic Kaiser-Bessel filter. That is not hard to understand when we realize that a 1 m/s radial velocity at 435 MHz represents only a 2.9 Hz Doppler shift. Based on a 0.85 s CPI, each Doppler filter is 1.2 Hz wide, and a 1 m/s target is in the second Doppler filter from the one containing DC clutter. For such small separations, the sharp filter cutoff provided by the rectangular filter provides significantly better, albeit unrealistic, performance, if its sidelobe effects are not included.

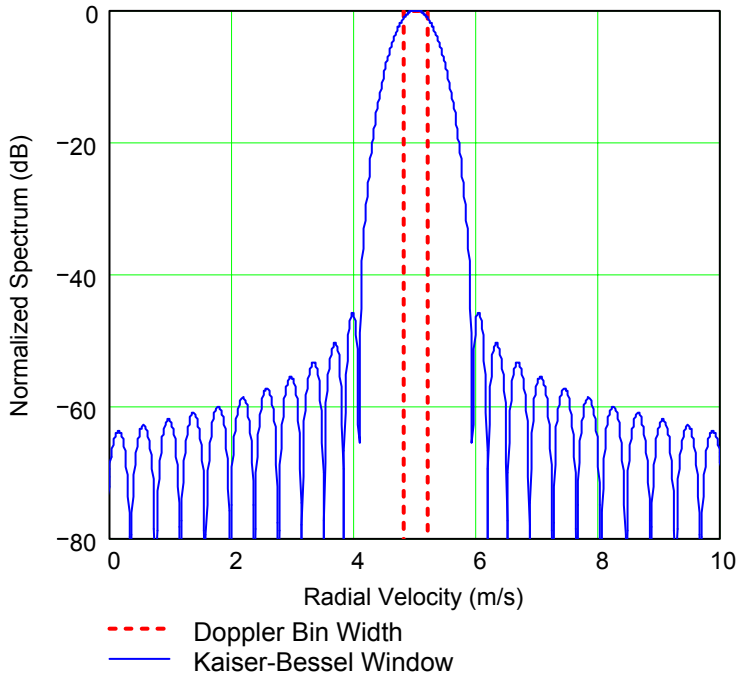

Figure 6. Comparison of the Kaiser-Bessel Window and Doppler Bin Width for the Strawman FOPEN GMTI System

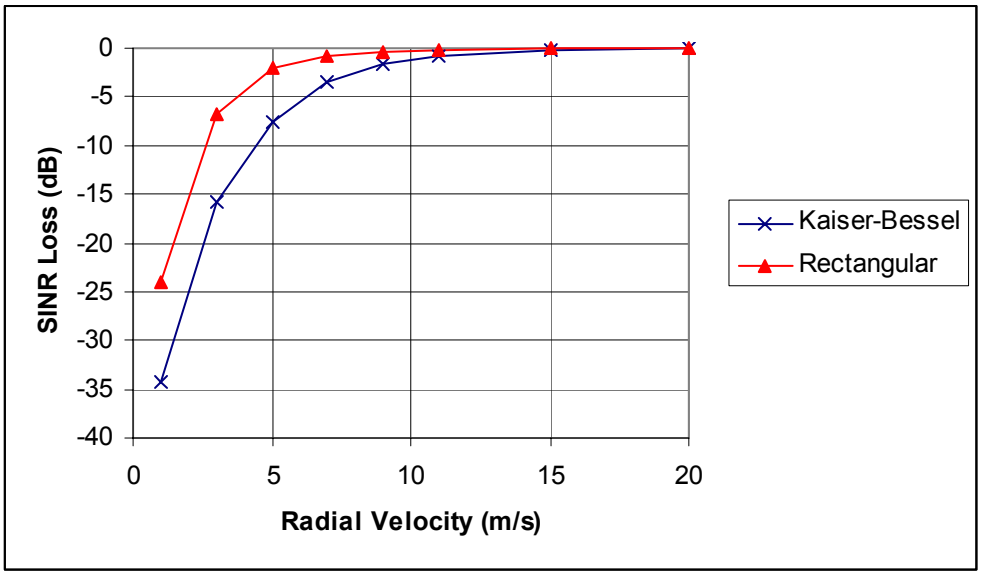

Figure 7. Predicted SINR Loss as a Function of Radial Velocity for the Strawman System and Two Doppler Filter Shapes

4.2.2 PRI-Staggered Processing

If a single DFT is performed on the data from the CPI, post-Doppler STAP provides spatial adaptivity only. As described by Ward (Ref. 18), several methods are available to insert temporal adaptivity and improve performance of a post-Doppler STAP processor. We have chosen to implement PRI-staggered processing. For this method, separate DFTs are performed on overlapping subsets of the pulses in the CPI. For example, if the CPI contains N pulses and an additional temporal DOF is desired, DFTs may be separately performed on pulses 1 through $N - 1$ and on pulses 2 through N, and adaptive weights calculated on that basis. More offset ("stagger") between the subsets may provide better performance. For instance, one stagger could use pulses 1 through $N - 5$ and the other pulses 5 through N. Similarly, more DOF can be generated by more pulse subsets, but at the expense of fewer pulses in each DFT. One disadvantage of implementing PRI-staggered processing is that it increases the number of DOF, and thus the processing burden; however, usually only two or three temporal DOF provide most of the benefit that can be derived from this technique, and so the increased processing is generally tolerable.

Thus, two variables must be explored regarding PRI stagger: how many staggers will be used and the number of pulses by which the staggers will be offset. The larger the number of staggers, the larger the number of DOF available for temporal adaptation. A larger number of staggers, however, effectively shortens the CPI of each stagger and broadens the Doppler filters within an individual stagger. For PRI stagger to provide independent information, the spatial looks within the staggers must be different from each other. That might argue for a large number of pulses between staggers; however, large numbers of pulses between staggers shortens the effective CPI of each stagger, again broadening the Doppler filters.

In exploring parameters for the strawman system, zero through three staggers were examined (providing one to four temporal DOF), as were one to five pulse offsets between staggers. The baseline parameters were chosen for the no-wind, no-scintillation case.

A significant improvement was seen going from no staggers to one stagger (approximately a 10-dB decrease in processing loss), an additional 1 dB was gained going from one to two staggers, and almost no improvement from two to three staggers (<0.4 dB). Two staggers, providing three temporal DOF, were chosen for the strawman.

Much less sensitivity to offsets between staggers was seen. The improvement in going from one pulse to five pulses between staggers was only 1.2 dB. This may not be surprising because the large satellite velocity (7,600 m/s) and low PRF (400 Hz) mean that in even a one-pulse offset, the antenna moves 19 m; however, because it provided somewhat improved performance, the five-pulse offset was used for the baseline predictions. That offset allows the antenna to move slightly less than its own length between the start of two adjacent staggers.

4.2.3 Clutter Internal Motion Model

The effect of internal clutter motion is to spread the clutter spectrum. This causes the area containing clutter that competes with the target to broaden, and thus a wider spatial null must be formed to cancel clutter competing with the target. Several models exist to model clutter internal motion. A Gaussian model historically has most often been used, although inverse-power-law models have also been fit to data (Ref. 21). More recently, Billingsley (Ref. 22) has made careful measurements of windblown clutter from trees and fit an exponential model to it. Billingsley's model, described below, is used in this effort.

The Billingsley model provides the power spectral density of windblown clutter as a function of frequency and wind speed. The spectrum is divided into two parts, with the total spectrum given as

$$P(v) = \frac{r}{r+1} \cdot \delta(v) + \frac{1}{r+1} \cdot P_{ac}(v) \quad , \tag{11}$$

where v is the Doppler velocity in meters per second, $\delta()$ is the Dirac delta function, r is a measure of the DC component of the spectrum, and $P_{ac}(v)$ is the AC component of the spectrum. The AC component is given by

$$P_{ac}(v) = \frac{\beta}{2} \cdot \exp(-\beta|v|) \quad , \tag{12}$$

where β is a constant that depends on the wind speed. The function r, which is used to apportion the total power between the AC and DC components, is given as (Ref. 22):

$$10\log_{10}(r) = -15.5\log_{10}(w) - 12.1\log_{10}(f) + 63.2 \quad , \tag{13}$$

with w the wind speed in miles per hour and f the radar frequency in megahertz.

Figure 8 provides an example spectrum from the model for the strawman carrier frequency of 435 MHz and a 20-mph wind. Again, the spectrum has been centered at a 5 m/s velocity for convenience.

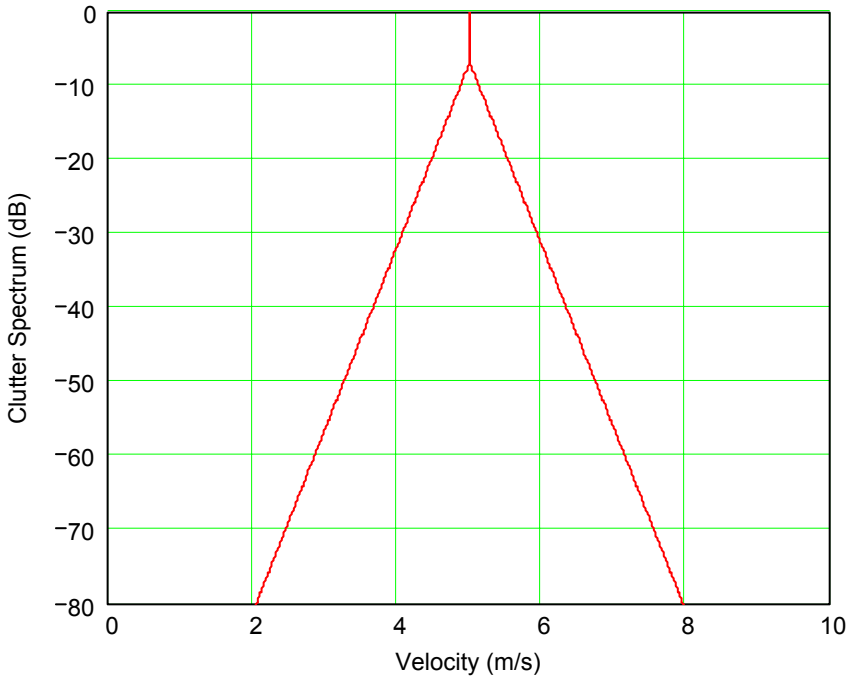

Figure 8. Clutter Spectrum for a 435-MHz Radar Frequency and 20-mph Wind Speed

4.2.4 FOPEN Loss Model

One of the substantial problems for FOPEN radar is providing sufficient radar resources to overcome the attenuation provided by propagation of the radar signal through foliage. To provide realistic results, an empirical model developed by Davis, et al. (Ref. 23), was added to the TechSat 21 framework. That model gives two-way attenuation as

$$\text{Two-Way Attenuation (dB)} = \beta F^{\alpha}(\sin 45°/\sin\gamma) \quad , \tag{14}$$

where β and α are constants that depend on polarization and on whether the median or 90th percentile is desired, F is the frequency in MHz, and γ is the grazing angle. Median horizontal polarization values of $\beta = 0.044$ and $\alpha = 0.79$ were chosen. At 435 MHz and 15-deg grazing, these values result in a two-way attenuation of 14.7 dB. To put foliage attenuation in perspective, that attenuation reduces the return from a 10 m^2 RCS target to that of a 0.34 m^2 target. Because the attenuation in decibels is proportional to the path length, in heavy foliage the loss rises rapidly with decreasing angle. Because the sine

function is essentially linear in the low-angle region, decreasing the grazing angle to 5 deg would triple the loss in decibels to approximately 44 dB, effectively increasing the loss by almost a factor of 1,000. Thus, it will be difficult for any FOPEN system operating at UHF to be effective at low grazing angles.

4.2.5 Scintillation Models

Scintillation spreads the spectrum of the clutter return similarly to internal clutter motion, but unlike clutter internal motion, it also decorrelates the target return, potentially reducing the effectiveness of coherent integration of the target signal. Both components of performance degradation were added to the TechSat 21 model. Each is discussed separately below, beginning with the effect of scintillation on the clutter spectrum.

Because the Mathcad framework being modified for this effort was constructed to look at post-Doppler processing and because a practical system would almost certainly employ such processing to reduce DOF to a manageable number, scintillation effects on clutter were implemented in the frequency domain. As noted earlier, scintillation temporal effects can be described in terms of the decorrelation properties of the signal mutual coherence function. Equation (2) notes that decorrelation data are well fit by a Gaussian function. This makes transforming the effects into the frequency domain simple, as a Gaussian function in the time domain transforms into another Gaussian in the frequency domain, with the result given by

$$S(f) = \frac{1}{\sqrt{2\pi}\cdot\sigma}\cdot\exp\left(\frac{-f}{2\sigma^2}\right) \quad , \tag{15}$$

where $\sigma = 1/\left(\sqrt{2}\cdot\pi\cdot\tau_o\right)$.

Section 5 discusses appropriate values for τ_0 at UHF under conditions of strong scintillation. Values of 0.1 s, 0.25 s, and 1.0 s are chosen as generally representative of points on the distribution of correlation times roughly corresponding to probabilities of occurrence of 1 percent, 10 percent, and 50 percent, respectively. Figure 9 provides the normalized spectra for those values of τ_0. Again, the spectrum has been centered at 5 m/s Doppler for convenience.

It is instructive to compare the spectrum caused by scintillation in Figure 9 with the Doppler filter width shown in Figure 6 and the windblown clutter spectrum of Figure 8. For Figure 6, the spectrum has a spread of not quite 2 m/s 40 dB below the peak. The windblown spectrum for 20-mph wind is slightly wider at that point, although it is substantially narrower than the Doppler filter spectrum above that point. The worst

case scintillation spectrum is much wider than either of the above, nearly 7 m/s at the –40 dB points. The nominal 10-percent point on the distribution, represented by $\tau_0 = 0.25$ s, is about the same width as the Doppler filter and windblown clutter spectra, while for $\tau_0 = 1$ s, the scintillation spectrum is significantly narrower than either of the others. Because the total clutter spectrum to be canceled is given by the convolution of the three components discussed, it is clear that scintillation will dominate in the worst cases, but will only marginally widen the total spectrum for τ_0 values greater than the CPI.

The second effect of scintillation is to decorrelate the target return. STAP analyses generally assume the target to be correlated over a CPI, and thus full coherent gain is available over that period. Based on Figure 9, it becomes obvious for the shorter decorrelation times that the return from the target will spread across more than one Doppler filter, thus reducing the integration gain. Knepp and Mokole (Ref. 2) provide an analysis of target coherent integration loss, L_{ci}, given by

$$L_{ci} = \frac{N + 2 \cdot \sum_{m=1}^{N-1} (N - m) \exp(-m^2 T^2 / \tau_0^2)}{N^2} \quad , \tag{16}$$

where N is the number of pulses in the CPI and T is the PRI.

Figure 10 provides a plot of coherent integration loss as a function of CPI length, with decorrelation time as a parameter for the same values of τ_0 used in Figure 9. The strawman system PRF of 400 Hz was used (PRI = 2.5 ms), but the PRF has very little influence on the loss as long as PRI$<<\tau_0$.

Note that for the 0.85 s CPI, target coherent integration loss ranges from as much as 7 dB to as little as a fraction of a decibel, depending on τ_0. For systems using SAR-type processing for GMTI, substantial losses could be incurred, even for relatively benign scintillation conditions. As an example, greater than 6 s integration time would be required to form a SAR image with a 10-m cross-range resolution. That results in greater than 5 dB loss in coherent target integration, even for a $\tau_0 = 1$ s.

The most elegant method for including scintillation loss in the STAP performance-prediction program would be in terms of a covariance matrix for the target. For this effort, a computationally simpler approach has been employed. That is, the target integration is assumed to provide the full coherent gain, and then a loss is included, based on Equation (16). The metric often applied to evaluate STAP is the SINR loss. As noted

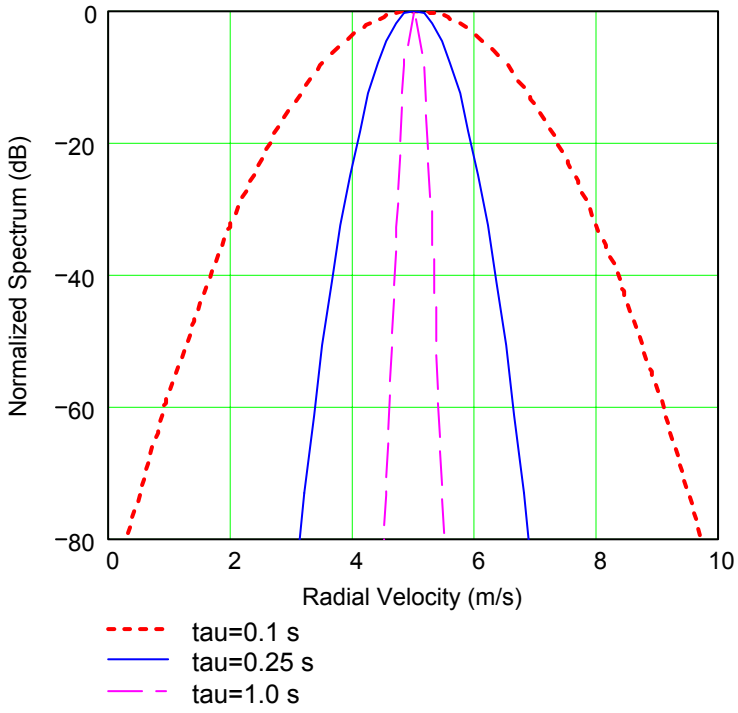

Figure 9. Normalized Ionospheric Scintillation Spectra for Representative Decorrelation Times

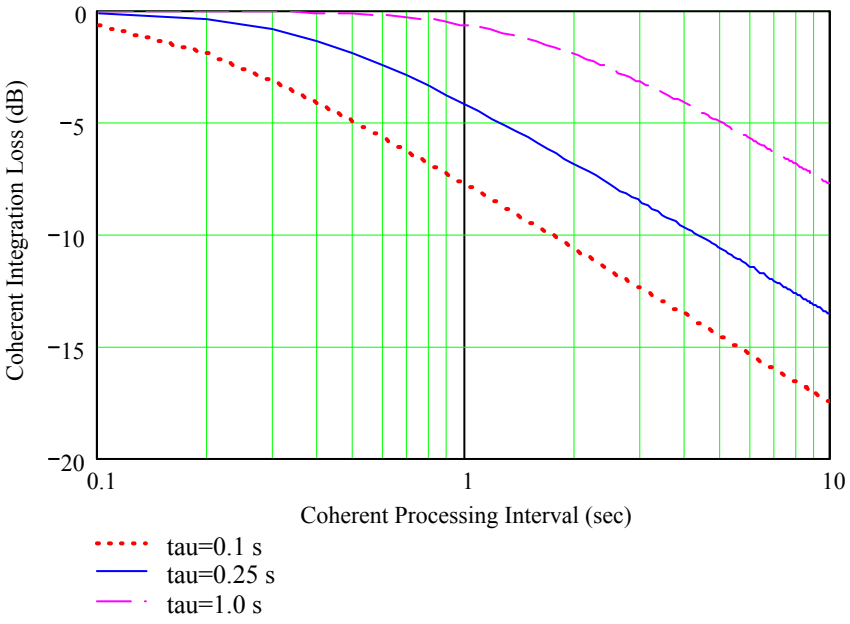

Figure 10. Target Coherent Integration Loss due to Ionospheric Scintillation as a Function of CPI for Three Representative Decorrelation Times

earlier, SINR loss is defined as the SINR after STAP compared with that available if the system was operating only against receiver noise. Thus, it is the loss caused by the signal processing to remove interfering clutter and jammers (not considered in this effort). For this effort, we have included the target coherent integration loss due to scintillation effects in the SINR loss.

4.3 IMPLEMENTATION OF STAP MODEL MODIFICATIONS

Implementation of the foliage-attenuation loss and loss in coherent target gain into the TechSat 21 program framework was simple. Each was included as a loss factor, although somewhat differently. The foliage-attenuation loss affects only the target signal. It has been implemented in the program as a factor multiplied by the actual target radar cross-section (RCS) to give an effective target RCS. Because foliage attenuation is not a signal-processing loss and is independent of scintillation, CPI length, STAP algorithm, etc., it is not included in the SINR loss.

Target coherent integration loss, on the other hand, is a loss incurred in signal processing. It is a function of the CPI length and the scintillation conditions. As noted above, to provide a complete picture of the losses provided by scintillation, it has been included as a signal-processing loss that appears as part of the SINR loss.

Providing for the PRI-staggered option in the STAP program is relatively straight-forward, albeit at the expense of increased computation time. As explained below where clutter contributions are discussed, the return from a particular clutter patch has a phase that is related to the range between the clutter patch and the antenna element being sampled. For the PRI-staggered case, in effect, multiple arrays are created, one for each of the staggers. The position of a given antenna element within each stagger will vary by the product of the satellite velocity and the time offset provided by the stagger. For the five-pulse stagger used for the strawman system, the offset of a given element between staggers is 95.2 m. Appropriate element offsets are used to calculate the phase for each of the elements for each of the staggers.

For the no-stagger case, the noise covariance matrix is diagonal. That is, the noise from element to element is considered uncorrelated. For the PRI-staggered case, that is no longer true. Although the covariance matrix elements describing the correlation between two different elements remain zero, the noise covariance of an element with itself on two different staggers is neither zero nor one because some—but not all—pulses are the same on two staggers. (Here, we have assumed the covariance of a given element

between staggers is given by the ratio of the common pulses in the two staggers divided by the total number of pulses in the stagger.)

The most complicated modification to the existing Mathcad program was the integration of Doppler filter, windblown clutter, and scintillation effects. The description of each provided above is in the terms of a frequency spectrum. The resulting spectrum is simply the convolution of the three individual spectra. Figure 11 provides an example of the convolved spectrum for the case of $\tau_0 = 0.25$ s and a 20-mph wind. Note that this is a case where the individual spectra contribute nearly equally to the convolved spectrum because they all have similar widths. For the worst case scintillation ($\tau_0 = 0.1$ s), however, scintillation dominates the spectrum, and the other components only marginally increase the spread. Examples of such cases are provided in Section 5.

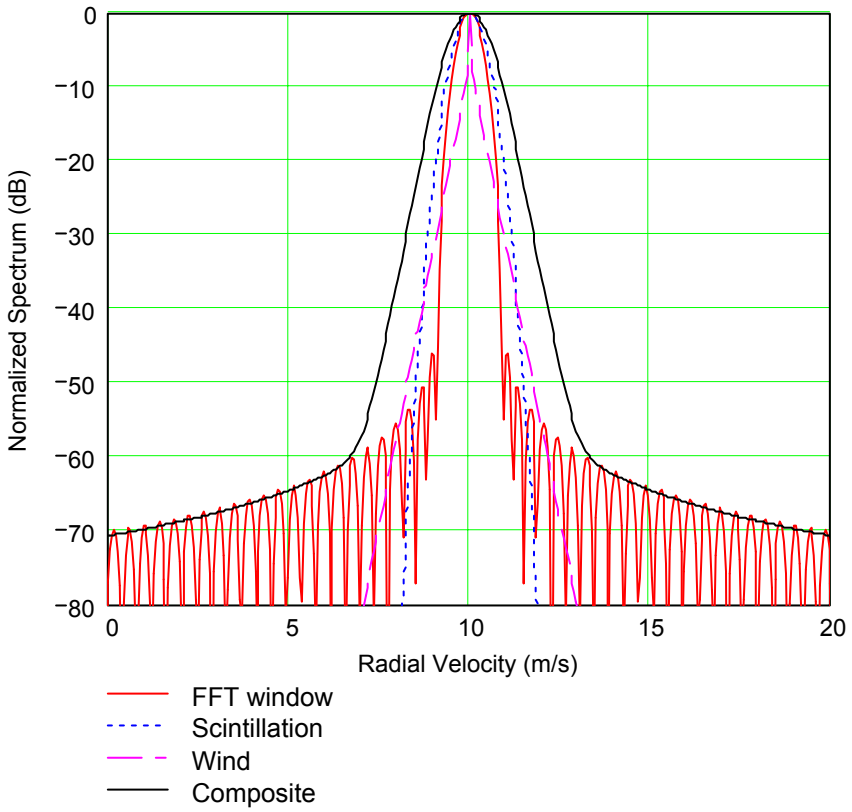

Figure 11. Example Spectrum for a Scintillation Decorrelation Time of 0.25 s, a Wind Speed of 20 mph, and a 0.85 s CPI

Calculating the convolved spectrum is only the first part of integrating the effects of the Doppler filter, scintillation, and wind on radar performance. The major effort is to correctly associate an amplitude and phase with a return from the ground in each element of the antenna array for each of the staggers. As noted earlier, the original Mathcad

program associated a single phase in each antenna element for the clutter area competing with the target. Every point on the ground can be associated with a particular Doppler frequency, based on its direction cosines relative to the satellite velocity vector. For a target with a radial velocity of 10 m/s, for example, there is a point on the ground forward of the satellite broadside, at the same range as the target, with an apparent Doppler of 10 m/s due to satellite motion. The range to that point will be slightly different for each of the antenna elements, resulting in a phase progression that becomes a factor in the clutter covariance matrix.

Thus, the focus of changes to the model to accurately reflect the effects of the Doppler filter window, windblown clutter, and ionospheric scintillation is to insert the correct clutter amplitude and phase into the clutter covariance matrix. The one-to-one correspondence between location and Doppler in the antenna mainbeam allows us to correctly fill the clutter covariance matrix. We have used a numerical technique, where the clutter competing with the target has been divided up into a number of small patches in azimuth. Empirical efforts have shown that steps in Doppler of 0.15 m/s, corresponding to azimuth angle steps of 1.26×10^{-3} degrees, are sufficiently small to give good results. This corresponds to slightly less than four steps across a Doppler filter width. The amplitude of the clutter return in each small patch is given as

$$\sqrt{\sigma_c} = \sqrt{\sigma_0 \cdot A_c \cdot G_t(\theta_a, \theta_i)} \cdot \left(\frac{R_{tgt}}{R_c} \right)^2 \cdot W(\theta_a, \theta_i) \quad , \tag{17}$$

where σ_c is the RCS of the clutter patch;

σ_0 is the clutter RCS per unit area;

A_c is the area of the clutter patch;

G_t is the transmit antenna gain in the direction of the patch (azimuth angle θ_a and incidence angle θ_i);

R_{tgt} and R_c are the range to the target and clutter patch, respectively (allowing for range ambiguous clutter); and

$W(\theta_a, \theta_i)$ is the spectral response, given as the convolution of the Doppler window, internal clutter motion, and scintillation spectra.

The amplitude from each patch will be the same for all of the subapertures, but the phase for each staggered subaperture, i, will be different and is given by

$$\phi_i = \frac{2\pi}{\lambda} \cos(\theta_a) \sin(\theta_i) \cdot d_i \quad , \tag{18}$$

where d_i is the position of the subaperture. The contribution of all patches to each subaperture is summed, and then the covariance matrix is calculated. The covariance matrix is inverted and used in the normal STAP manner to calculate complex weights for the DOF available.

In theory, the spectral extent of the clutter interfering with the target goes from plus the platform velocity to minus the platform velocity. As Figure 11 shows, however, the spectrum drops off very rapidly. Even for the shortest ionospheric decorrelation time explored (0.06 s) and with a 20-mph wind, the convolved spectrum is down 60 dB within ±7.5 m/s of the center velocity. For this effort, a region ±12 m/s around the patch having the same Doppler as the target was used for summing clutter effects. Limited tests of wider windows indicated that very little change in STAP loss (<1 dB) was seen.

5. RESULTS

The modifications to the Mathcad STAP model are intended to include the effects that would be important in performance of a space-based FOPEN GMTI system. The approach taken to evaluate the effect of scintillation on performance is through a straw-man SBR system. The next subsection provides parameters for the strawman system and explains how they are chosen. Section 5.2 explores scintillation decorrelation properties in the strawman's UHF band. Section 5.3 provides results documenting the effects on performance of scintillation alone and of scintillation combined with clutter internal motion.

5.1 STRAWMAN SYSTEM PARAMETERS

A number of different approaches are available to evaluate the effects of scintillation on the performance of a FOPEN GMTI system operating from space. Based on the results presented in Figure 10, long coherent integration times would provide significant integration loss for systems using SAR-like processing. For that reason, such concepts were not explored further. If reasonably short CPIs are chosen, clutter cancellation becomes a major concern, and that leads directly to the choice of STAP for the system-processing architecture. Rather than attempting to produce generalized STAP results, we have chosen to postulate a system that meets reasonable performance requirements without scintillation and then to calculate the effects of scintillation on performance. Table 1 provides the parameters chosen.

The basic approach taken is to postulate the performance parameters [probability of detection (Pd), probability of false alarm (pfa), and minimum detectable velocity (MDV)] and then arrive at a reasonable set of system parameters that meets performance requirements with no scintillation or clutter internal motion. The UHF frequency band is chosen because it has a radar frequency allocation and is likely the highest frequency available to a radar that permits reasonable FOPEN. Other parameters are chosen as reasonable and representative. To substantiate the choices made, some of the perform-ance requirements and the system parameters are discussed below.

Table 1. Strawman System Parameters

Parameter	Value
Altitude (km)	500
Minimum Detectable Velocity (m/s)	3
Minimum Grazing Angle (degrees)	15
Probability of Detection	0.9
Probability of False Alarm	1×10^{-6}
CPI (s)	0.85
CPI/Dwell	2
Target Fluctuation	Swerling II
STAP	Element Space, Post Doppler
Center Frequency (MHz)	435
Antenna Size (m)	110×30
Average Transmit Power (kW)	1
IF Bandwidth (MHz)	15
Noise Figure (dB)	2
Losses (dB)	10 + Foliage + STAP
Target RCS (dBsm)	10

An LEO satellite is chosen to minimize the radar assets required for an individual radar (although, not, perhaps, the assets for an entire operational system). In the same vein, 500 km is toward the lower side of practical LEO altitudes, again minimizing required individual radar assets. For a given required revisit time, however, such low altitudes imply much larger constellations of satellites than would be required for middle, high, or geosynchronous orbits.

An MDV of 5 km/hr is a typical specification for a GMTI system. That corresponds to a 1.4-m/s radial velocity. MDVs above 3 m/s are generally judged to have significant operational disadvantages, particularly because only a fraction of a target's velocity is likely to be radial. Because of the extreme losses a UHF GMTI system will experience at very low target velocities, the 3-m/s MDV value has been chosen here for system sizing. Recognize, however, that some in the operational community might judge 3 m/s to be inadequate.

The minimum grazing angle of 15 deg is a strong driver on system performance for several reasons. First, minimum grazing angle determines maximum range. For this satellite altitude, the slant range to a target at 15-deg grazing is 1,407 km. Decreasing the minimum grazing angle to 10 deg increases the slant range to 1,695 km, thereby

decreasing the target signal by a little more than 3 dB. More important, the foliage attenuation goes from 14.7 dB to 20 dB, decreasing the target signal by a further 5.3 dB. Table 2 illustrates the tradeoffs involved with grazing angle. Note that for the strawman system parameters, a substantial Pd is achieved only for grazing angles between 10 deg and 60 deg, with only 15–45 deg showing Pd values in the vicinity of 0.9. Driving performance to a higher Pd at lower angles would be difficult because of the combination of R^{-4} effects and foliage attenuation. At the higher angles, STAP losses increase because of increasing clutter power, which requires deeper STAP spatial nulls to drive clutter power down to noise power. That situation could be improved by increasing the bandwidth to narrow the clutter cell. However, only 30 MHz of bandwidth is available to radars at UHF. If that is all used to reduce clutter size, frequency hopping would not be available to decorrelate target returns from CPI to CPI. In any event, for the strawman system parameters, a Pd $\geq$ 0.9 could be delivered over a swath about 850 km wide.

Table 2. Example Performance for the Strawman System with no Scintillation or Clutter Internal Motion

Grazing Angle (deg)	Ground Range (km)	Foliage Atten. (dB)	Prob. of Detection
1	2,414	218.6	0
5	2,017	43.8	0
10	1,620	22.0	0.44
15	1,316	14.7	0.90
20	1,083	11.2	0.95
30	760	7.6	0.95
35	644	6.7	0.94
45	465	5.4	0.89
60	275	4.4	0.60
70	174	4.1	0.20

Note again that the Pd values in Table 2 are for the case of no scintillation and no windblown clutter. Thus, they represent a baseline against which we can evaluate the effects of scintillation and the combination of scintillation and internal clutter motion on performance.

The most challenging portion of the strawman system is the 3,300 m^2 antenna (110 m $\times$ 30 m) it requires. In addition to the mechanical and electrical challenges of designing and manufacturing such an antenna, there is an additional concern for its longevity because of the potential rate of impacts by meteoroids and manmade space debris. Thus, it is worthwhile to discuss the factors that drove its sizing and explore

possible trade-offs that might reduce its area. Note that in all the cases investigated, the radar is clutter limited (that is, interference is dominated by clutter, rather than noise) and would be able to detect a 10 m^2 target in noise, even accounting for foliage attenuation. Thus, if sufficient clutter suppression were available with no additional loss, antenna size could be reduced.

The height of the antenna is sized so that range ambiguities with the antenna beam centered at 90-deg azimuth (broadside) and 15-deg grazing are outside the transmit antenna elevation mainbeam nulls for the 400-Hz PRF chosen. The 400-Hz PRF is chosen to keep Doppler ambiguities outside the transmit antenna azimuth mainbeam nulls for the antenna length. A one-parameter, Taylor, azimuth and elevation taper, providing –25 dB first sidelobes, is used on transmit. A uniform taper would allow antenna size to be reduced, but at the expense of additional STAP DOF to cancel sidelobe clutter (and likely the use of elevation-plane STAP). Also, since the radar is clutter limited, operating with the peak of the transmit beam squinted to a larger grazing angle than the minimum would allow some reduction in antenna height. Even with optimization, however, a very large antenna will be required.

5.2 SCINTILLATION DECORRELATION PARAMETERS

Because the purpose of this effort is to evaluate scintillation effects on SBR FOPEN GMTI performance, the focus is on cases where scintillation is severe enough to cause an effect. For that reason, near-equator scintillation data form the basis of the statistics used. Nevertheless, both worst case and less severe case scintillation data are included in the parameter space explored.

As noted in Section 3.2, the Wideband Satellite experiment provided data from Kwajalein and Ancon, Peru, for a period of high solar activity in 1979 and for a period of significantly less solar activity in 1977. Knepp and Mokole (Ref. 2) give cumulative distributions for τ_0 for both periods for the one-way decorrelation time. They also assert that

$$\tau_{2-\text{way}} = \frac{\tau_{1-\text{way}}}{\sqrt{2}} \quad , \tag{19}$$

where $\tau_{2\text{-way}}$ and $\tau_{1\text{-way}}$ are the two-way and one-way decorrelation times, respectively. Based on the distributions in Ref. 2 and Equation (19), Table 3 provides decorrelation times for Ancon, Peru, in February–April 1997 and for Kwajalein during June–July 1979. Note that although decorrelation times are the same at the 0.1-percent point on the distributions for the two locations, decorrelation times for Ancon during less severe solar

activity are longer for all the other cases. The data records from which decorrelation times were calculated were only 8.192 s long. Thus, two-way decorrelation times longer than 5.8 s cannot be calculated, and there is likely some inaccuracy at the longer decorrelation times because of the few overlapping points available for calculations at the long lag times. Nevertheless, values at the 50-percent point on the cumulative distribution should be accurate.

Table 3. Two-Way Decorrelation Values for Two Times and Locations from Ref. 2

Probability ($\tau \leq$ value)	Ancon, 1977	Kwajalein, 1979
0.1 %	0.06 s	0.06 s
1.0 %	0.12 s	0.08 s
10 %	0.33 s	0.13 s
50 %	2.12 s	0.67 s
90 %	>5.8 s	>5.8 s

The decorrelation times in Table 3 are representative of the worst that might be seen under two different conditions of solar activity. Rather than pick either set or do extensive calculations for both sets, we have chosen nominal values of decorrelation for strawman system calculations. A value of 0.1 s was chosen as representative of very severe scintillation (near the 1-percent point on the distribution). Values of 0.25 s and 1.0 s were the other values chosen as generally representative of the 10-percent and 50-percent points, respectively, on the distribution. Those three values provide a range of severe scintillation effects that span what might be expected for a FOPEN GMTI system.

5.3 SCINTILLATION AND CLUTTER INTERNAL MOTION RESULTS

Figure 12 illustrates the basic effects of scintillation alone on strawman system performance. SINR loss for three values of scintillation decorrelation is plotted as a function of target radial velocity. System parameters are as provided in Table 1.

As a point of reference, the result for τ_0 = 1.0 s at 3 m/s radial velocity is only about 1 dB worse than for the case with no scintillation, which the simulation predicts to show 15.7 dB of SINR loss. Of that 1 dB degradation, 0.5 dB is target integration loss and 0.5 dB is additional clutter cancellation loss. Thus, scintillation decorrelation times longer than the CPI should have little effect on a system using a realistic Doppler window.

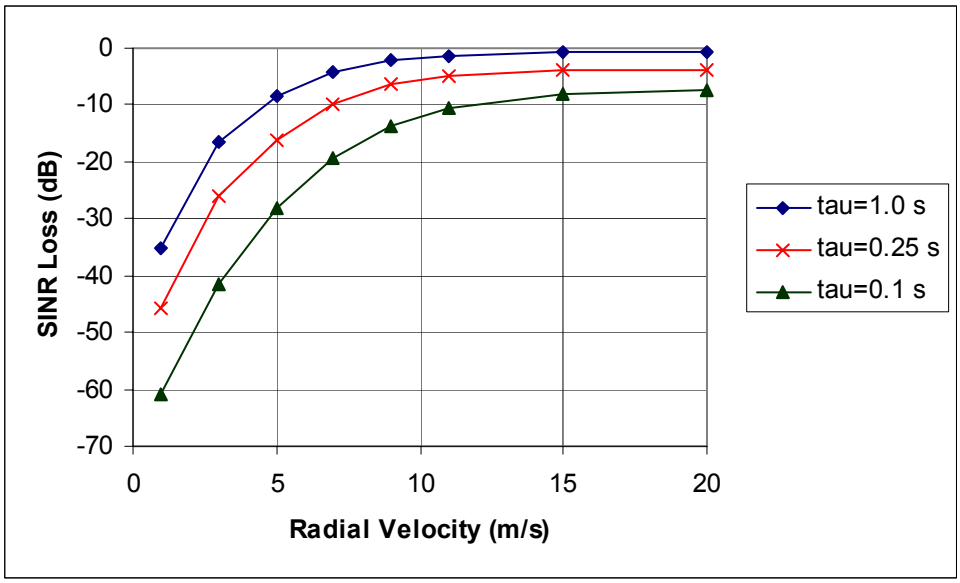

Figure 12. SINR Loss as a Function of Radial Velocity for the Strawman System with Decorrelation Time as a Parameter

In examining performance, we found that for the CPI chosen, the spectral width of the Doppler filter dominated SINR loss for the longer decorrelation times. The additional SINR losses provided by scintillation with $\tau_0 = 1.0$ s and by internal clutter motion for a wind speed of 20 mph are similar, as shown in Figure 13, which plots the SINR

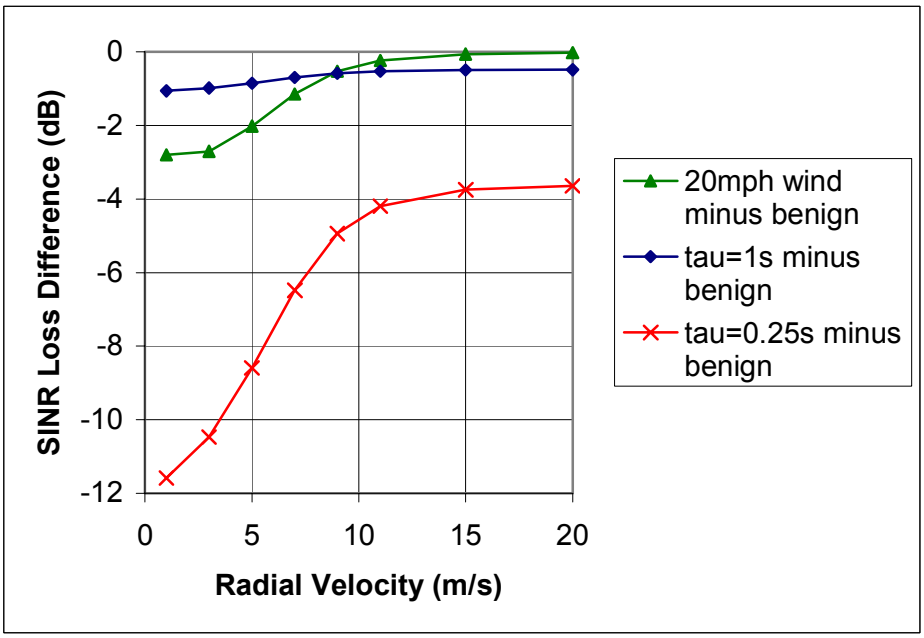

Figure 13. SINR Loss Difference Caused by Clutter Internal Motion for a 20-mph Wind, for Scintillation with a 1-s Decorrelation Time, and for Scintillation with a 0.25-s Decorrelation Time

loss difference between the benign case (no scintillation or clutter internal motion) and cases of wind alone or scintillation alone. The difference between the two curves at the higher radial velocities is the 0.5-dB target integration loss caused by scintillation, but not in effect for windblown clutter.

Note that reducing the correlation time to 0.25 s, however, increases the SINR loss significantly over what would be seen with a 20-mph wind. A little over 3.5 dB of the loss can be attributed to target integration loss. Thus, although a 1-s decorrelation time does not markedly compromise strawman system performance, reducing the decorrelation time to 0.25 s does, even for large target radial velocities.

Given that the effects of a 20-mph wind and 1.0-s scintillation decorrelation time are similar, we explore the effects of the combination. Figure 14 provides predictions of SINR loss difference from the case of a 20-mph wind and no scintillation to one with both a 20-mph wind and scintillation with a 1.0-s decorrelation time. The results indicate that only marginal additional loss is incurred, about 0.9 dB at a 3-m/s target radial velocity. This reduces Pd from 0.75 with a 20-mph wind alone to 0.68 with a 20-mph wind and scintillation added.

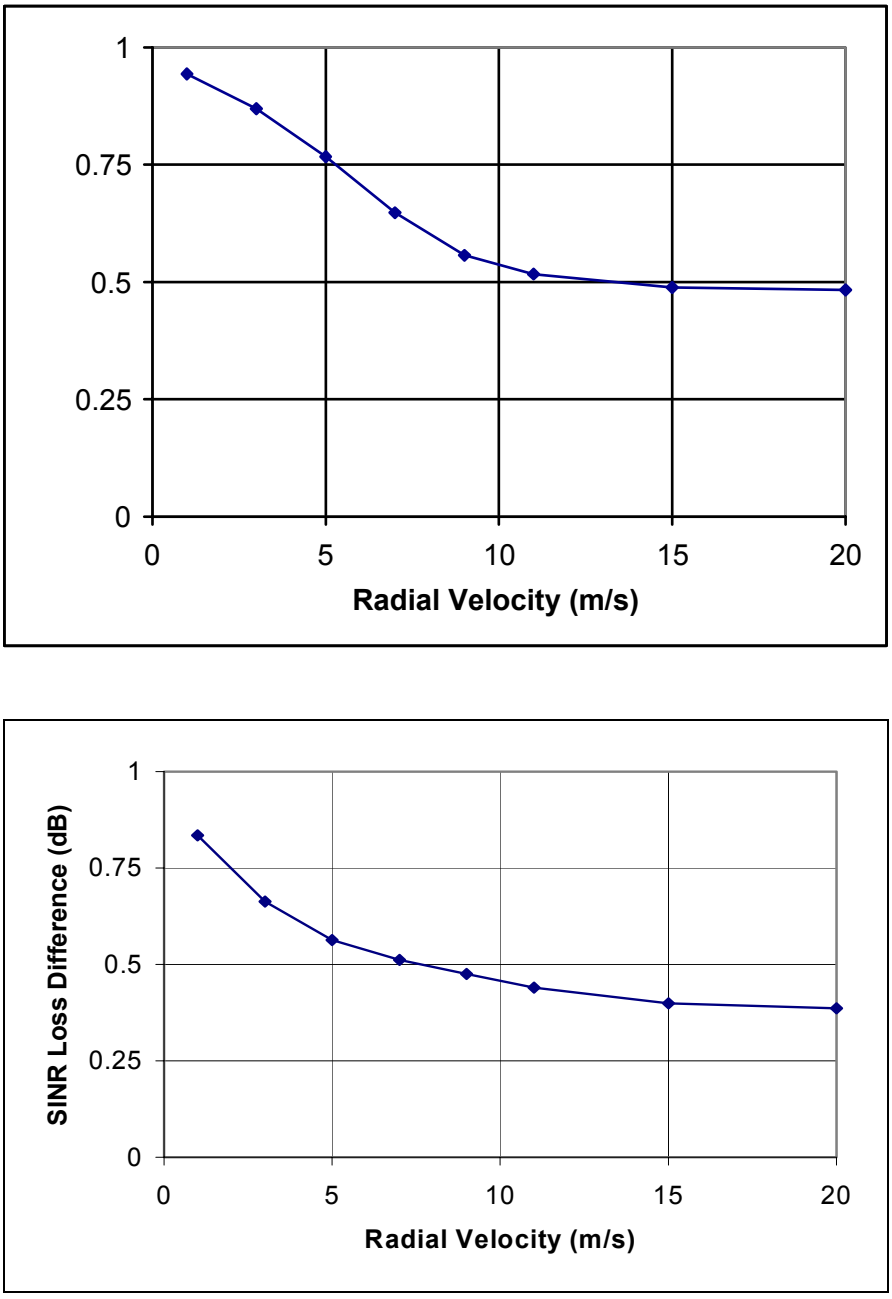

Figure 14. Additional SINR Loss Provided by Scintillation with a Decorrelation Time of 1.0 s (bottom) over that for a 20-mph Wind and no Scintillation (top)

6. CONCLUSIONS

The effects of ionospheric scintillation on an FOPEN SBR performing GMTI have been studied through the use of a strawman system design. The baseline system is sized to achieve a 0.9 probability of detection through foliage with a 1×10^{-6} probability of false alarm at 15-deg grazing. A 10-m^2 target having a radial velocity of 3 m/s is assumed. STAP is used to provide cancellation of clutter that would compete with the target.

Achieving the baseline performance requires a system with a 110 m × 30 m antenna and 1 kW average transmitted power. The large power-aperture product is necessary for several reasons. First, the long detection ranges forced by the space geometry result in large R^4 losses (246 dB at 15-deg grazing) that must be overcome with a combination of power, aperture, and coherent integration. However, available coherent integration will be limited if operation during scintillation is desired. Next, foliage attenuation at this grazing angle reduces the target signal by almost 15 dB. Finally, the target and the clutter with which it competes are very close to each other in angle because of the low target radial velocity and the high speed of the satellite. This proximity causes a very large signal-processing loss to be incurred when a spatial null is formed to cancel the clutter (approximately 15 dB for the 3 m/s target). This combination of factors will drive the assets required for any radar designed for this mission.

Severe ionospheric scintillation seen in Earth's equatorial regions (nominally the 1-percent and 10-percent points on the cumulative distribution) significantly degrades strawman system performance. For the 3-m/s radial velocity used as a benchmark, an additional 26 dB of SINR loss is seen for the 1-percent decorrelation time, and 10 dB additional loss is seen for the 10-percent case. Performance degradation is caused by a combination of decreased efficiency in coherently integrating the target signal and an increase in the width of the angle over which clutter that competes with the target must be cancelled. Performance degradations from scintillation would generally be less severe in the polar regions and likely would be inconsequential in the mid-latitudes (20–50 deg).

Under normal conditions, other processing techniques, such as SAR-based GMTI or wideband operation, could potentially reduce the radar resources required, but at the expense of additional processing and reduced coverage rate. If SAR processing is used,

however, the system must be able to operate successfully in the face of much larger target-integration losses than occur for the strawman with its STAP implementation. FOPEN requirements drive the design toward UHF frequencies, and insufficient bandwidth is available at UHF to make use of wideband techniques to reduce clutter very attractive. In addition, coherence bandwidths at UHF under severe scintillation conditions are limited to about 30 MHz, further impeding the use of wideband coherent systems.

In summary, implementation of a space-based, FOPEN, GMTI radar appears to require extremely large power-aperture products, even in a benign environment. The addition of ionospheric scintillation drives the radar toward resource requirements that might not be achievable. As noted, however, scintillation is a strong function of location, time of day, and season. Thus, a careful study of operational requirements would be required to define the ionospheric scintillation conditions under which a system might have to perform.

GLOSSARY

AFRL	Air Force Research Laboratory
C/NOFS	Communication/Navigation Outage Forecasting System
CPI	coherent processing interval
DFT	discrete Fourier transform
DNA	Defense Nuclear Agency
DOF	degrees of freedom
FOPEN	foliage penetration
GMTI	ground moving-target indication
HAARP	High Frequency Active Auroral Research Program
HF	high frequency
IDA	Institute for Defense Analyses
LEO	low-Earth orbit
LOS	line of sight
MDV	minimum detectable velocity
NWRA	Northwest Research Associates
ONR	Office of Naval Research
Pd	probability of detection
PEAK	Propagation Effects Assessment—Kwajalein
PRF	pulse-repetition frequency
PRI	pulse-repetition interval
RCS	radar cross-section
SAR	synthetic aperture radar
SBR	space-based radar
SCINDA	Scintillation Network Decision Aid
SINR	signal-to-interference-plus-noise ratio
STAP	space-time adaptive processing
UHF	ultrahigh frequencies
VHF	very high frequencies

REFERENCES

1. Knepp, D.L., J.T. Reinking, "Radar Detection During Scintillation," DTIC ADA220099, 1990.

2. Knepp, D.L., E.L. Mokole, "Space-Based Coherent Processing During Scintillation: VHF Through L-band," *Radio Science*, **27** (1), 47–61, 1992.

3. Fremouw, E.J., et al., "On the Statistics of Scintillating Signals," *Journal of Atmospheric and Terrestrial Physics*, **42**, 717–731, 1980.

4. Knepp, D.L., "Analytic Solution for the Two-Frequency Mutual Coherence Function for Spherical Wave Propagation," *Radio Science*, **18** (4), 535–549, 1983.

5. Jursa, A.S., ed., *Handbook of Geophysics and the Space Environment*, Air Force Geophysics Laboratory, 10-71 through 10-88, 1985.

6. Aarons, J., "Global Morphology of Ionospheric Scintillations," *Proc. IEEE,* **70**, 360–378, April 1982.

7. Bramley, E.N., "Fluctuations in Direction and Amplitude of 136 MHz Signals from a Geostationary Satellite," *J. Atmos. Terr. Phys.*, **36**, 1503–1513, 1974.

8. Livingston, R.C., "Comparison of Multifrequency Equatorial Scintillation: American and Pacific Sectors," *Radio Science*, **15** (4), 801–814, 1980.

9. Basu, S., et al., "Comparison of Ionospheric Scintillation Statistics from the North Atlantic and Alaskan Sectors of the Auroral Oval Using the Wideband Satellite," DTIC AD A111871, 1981.

10. McHwain, C.E., "Coordinates for Mapping the Distribution of Magnetically Trapped Particles," *J. Geophys. Res*., **66**, 3681, 1961.

11. Rino, C.L., et al., "Wideband Satellite Observations," DTIC AD A048801, 1977.

12. Knepp, D.L., E.L. Houpis, "VHF/UHF Radar Scintillation Effects Observed by Altair," DTIC AD P006290*,* 1990.

13. Secan, J.A., R.M. Bussey, E.J. Fremouw, S. Basu, "High-Latitude Upgrade to the Wideband Ionospheric Scintillation Model," *Radio Science*, **32** (4), 1567–1574, 1997.

14. Fremouw, E.J., C.L. Rino, "An Empirical Model for Average F-Layer Scintillation at VHF/UHF*,*" *Radio Science*, **8** (3), 213–222, 1973.

15. Fremouw, E.J., J.A. Secan, "Modeling and Application of Scintillation Results," *Radio Science*, **19** (3), 6878–694, 1984.

16. Secan, J.A., R.M. Bussey, "An Improved Model of High-Latitude F-Region Scintillation (WBMOD Version 13)," DTIC AD A288558, 1994.

17. Secan, J.A., R.M. Bussey, E.J. Fremouw, "An Improved Model of Equatorial Scintillation," *Radio Science*, **30** (3), 607–617, 1995.

18. Ward, J., "Space-Time Adaptive Processing for Airborne Radar," MIT Lincoln Laboratory Technical Report 1015 (ESC-TR-94-109), 13 December 1994.

19. Miller, R.W., "Space-Time Adaptive Processing for TechSat 21 MTI Radar," Air Force Research Laboratory, May 1999.

20. Harris, F.J., "On the Use of Windows for Harmonic Analysis with the Discrete Fourier Transform," *Proc. IEEE*, **66**, 51–83, January 1978.

21. Long, M.W., *Radar Reflectivity of Land and Sea,* Artech House, Boston, 156–158, 1983.

22. Billingsley, J.B., "Exponential Decay in Windblown Radar Ground Clutter Doppler Spectra: Multifrequency Measurements and Model," MIT Lincoln Laboratory Technical Report 997 (ESC-TR-95-098), 29 July 1996.

23. Davis, M., P. Tomlinson, R. Maloney, "Technical Challenges in Ultra-Wideband Radar Development for Target Detection and Terrain Mapping," *Proceedings of the IEEE 1999 National Radar Conference*, Boston, MA, April 20–22, 1999.

24. Knepp, D.L., R.A. Dana, "The Impact of Strong Scintillation on Space-Based Radar Design: Clutter Rejection," *Radar Science*, **20** (3), 366–374, May-June 1985.

REPORT DOCUMENTATION PAGE

Form Approved
OMB No. 0704-0188

1. REPORT DATE	2. REPORT TYPE	3. DATES COVERED *(From–To)*
August 2001	Final	March 2000 – February 2001

4. TITLE AND SUBTITLE
Ionospheric Scintillation Effects on a Space-Based, Foliage-Penetration, Ground Moving Target Indication Radar

5a. CONTRACT NUMBER
DAS W01 98 C 0067

5b. GRANT NUMBER

5c. PROGRAM ELEMENT NUMBER

6. AUTHOR(S)
M.T. Tuley, T.C. Miller, R.J. Sullivan

5d. PROJECT NUMBER

5e. TASK NUMBER
DA-2-155

5f. WORK UNIT NUMBER

7. PERFORMING ORGANIZATION NAME(S) AND ADDRESS(ES)
Institute for Defense Analyses
4850 Mark Center Drive
Alexandria, VA 22311-1882

8. PERFORMING ORGANIZATION REPORT NUMBER
IDA Document D-2579

9. SPONSORING / MONITORING AGENCY NAME(S) AND ADDRESS(ES)
DARPA/TTO
3710 N. Fairfax Drive
Arlington, VA 22203-1714

10. SPONSOR/MONITOR'S ACRONYM(S)

11. SPONSOR/MONITOR'S REPORT NUMBER(S)

12. DISTRIBUTION / AVAILABILITY STATEMENT
Approved for public release; distribution unlimited.

13. SUPPLEMENTARY NOTES

14. ABSTRACT

This report provides the results of a brief study of the possible effects of ionospheric scintillation on a space-based, foliage-penetration (FOPEN), ground moving-target indication (GMTI) radar operating in the ultrahigh-frequency (UHF) band. The results of publicly available data and analyses are applied to a specific strawman FOPEN space-based radar (SBR) system operating from low-Earth orbit. Performance degradations due to ionospheric scintillation and a combination of ionospheric scintillation and internal clutter motion caused by wind are calculated for a 3 m/s target minimum detectable velocity (MDV) at 15-deg grazing, point parameters felt to be minimally acceptable for an operational system. Space-time adaptive processing (STAP) is used to provide the clutter rejection necessary for successful performance. Implications of ionospheric scintillation for synthetic aperture-based GMTI processing are also discussed.

15. SUBJECT TERMS
space-based radar, GMTI radar, ionospheric scintillation, space-time adaptive processing (STAP)

16. SECURITY CLASSIFICATION OF:			17. LIMITATION OF ABSTRACT	18. NUMBER OF PAGES	19a. NAME OF RESPONSIBLE PERSON
					Mr. Lee Moyer
a. REPORT Uncl.	b. ABSTRACT Uncl.	c. THIS PAGE Uncl.	SAR	54	19b. TELEPHONE NUMBER *(include area code)* 703-248-1514

Standard Form 298 (Rev. 8-98)
Prescribed by ANSI Std. Z39.18